Phase transitions and spatially ordered counterion association in ionic-lipid membranes: A statistical model

M. N. Tamashiro[*]

Instituto de Física "Gleb Wataghin" , Universidade Estadual de Campinas — UNICAMP, 13083-970, Campinas, SP, Brazil

C. Barbetta, R. Germano,[†] and V. B. Henriques[‡]

Instituto de Física, Universidade de São Paulo, Caixa Postal 66318, 05314-970, São Paulo, SP, Brazil

We propose a statistical model to account for the gel-fluid anomalous phase transitions in charged bilayer- or lamellae-forming ionic lipids. The model Hamiltonian comprises effective attractive interactions to describe neutral-lipid membranes as well as the effect of electrostatic repulsions of the discrete ionic charges on the lipid headgroups. The latter can be counterion dissociated (charged) or counterion associated (neutral), while the lipid acyl chains may be in gel (low-temperature or high-lateral-pressure) or fluid (high-temperature or low-lateral-pressure) states. The system is modeled as a lattice gas with two distinct particle types—each one associated, respectively, with the polar-headgroup and the acyl-chain states—which can be mapped onto an Ashkin-Teller model with the inclusion of cubic terms. The model displays a rich thermodynamic behavior in terms of the chemical potential of counterions (related to added salt concentration) and lateral pressure. In particular, we show the existence of semidissociated thermodynamic phases related to the onset of *charge order* in the system. This type of order stems from spatially ordered counterion association to the lipid headgroups, in which charged and neutral lipids alternate in a checkerboard-like order. Within the mean-field approximation, we predict that the acyl-chain order-disorder transition is discontinuous, with the first-order line ending at a critical point, as in the neutral case. Moreover, the charge order gives rise to continuous transitions, with the associated second-order lines joining the aforementioned first-order line at critical end points. We explore the thermodynamic behavior of some physical quantities, like the specific heat at constant lateral pressure and the degree of ionization, associated with the fraction of charged lipid headgroups.

I. INTRODUCTION

Amphiphile molecules in solution spontaneously self-assemble in several supramolecular aggregates, such as micelles, lamellar and hexagonal phases, and unilamellar or multilamellar vesicles. Aqueous suspensions of vesicles formed by zwitterionic (neutral) phospholipids—such as PC (phosphatidylcholine)—present a gel-fluid transition, associated with the disordering of the lipid acyl chains, usually called the main transition [1]. This phase transition is sharp, with a latent specific heat and discontinuity in the thermodynamic properties of the suspension, being thus classified as a first-order transition. Several experimental techniques, such as small-angle x-ray scattering (SAXS) [2–5], electronic spin resonance (ESR) [6–8], fluorescence spectroscopy [9], light scattering [10–12], electron microscopy [13–15], optical microscopy of giant vesicles [3,4,11] and differential scanning calorimetry (DSC) [11–17], point out that the main transition in the case of lipids containing polar headgroups that may undergo ionic dissociation, such as PG (phosphatidylglycerol) [18], may be broadened, depending on acyl-chain length,

lipid concentration, pH, and ionic strength. For low salt concentration, this transition region is wide in the case of lipids of shorter acyl-chain lengths, such as DMPG (=14 carbon diacyl saturated chains [19]), whereas for lipids of longer chains, such as DPPG, it turns very narrow [14,20–22] and disappears completely for longer chains still, as in the case of DSPG (18 carbon atoms long). Moreover, the usual sharp gel-fluid transition of zwitterionic lipids is recovered on addition of sufficient amount of monovalent salt [14,18,23–27].

This broad transition region, with a smoothened specific-heat profile, was called intermediate or anomalous transition region. Although this region and its associated thermodynamic phase is still under investigation, aqueous suspensions formed by ionic short-chain lipids present some remarkable properties such as low turbidity [10,11], high electrical conductivity [10,17], and high viscosity [14,17] in the anomalous transition region. In particular, at the onset of the main transition region, one observes a discontinuous rise of the conductivity [10,17] and viscosity [14,17] of the suspension—which clearly indicates to be thus a first-order transition—followed by a smooth increase and eventually a steep (but apparently continuous [17]) falloff at the end of the transition region. Despite several attempts [3,9,11,14,28] to explain this peculiar behavior, the underlying microscopic origin at the molecular level has not yet been fully established. Certainly, this complex behavior stems from the competition between several intramolecular interactions of the lipid molecules mediated by the aqueous solvent.

---

[*]mtamash@ifi.unicamp.br

[†]Present address: Departamento de Física, Universidade Federal do Piauí, Centro de Ciências da Natureza, Campus Universitário Ministro Petrônio Portella, Ininga, 64049-550, Teresina, PI, Brazil.

[‡]vera@if.usp.br

Other anionic lipid systems, such as DPPS at high pH and phosphatidic acid (PA), also show a gradual gel-fluid phase transition, which earlier was attributed to the presence of a mixed phase $L_{\alpha\beta}$ (coexisting gel-fluid) between the conventional L_α (fluid lamellar) and the L_β (gel lamellar) phases [29]. Furthermore, at the mesoscopic length scales, the lipid aggregates may undergo structural transitions, probably due the nontrivial coupling among the long-ranged electrostatic interactions, bilayer flexibility [30], and undulation fluctuations [31]. It should be noted that a theoretical study accounting for Coulomb interactions between charges and short-ranged interactions between hydrophilic and hydrophobic lipid moieties, as well as between charges and solvent [32] is able to explain the lyotropic phases observed in zwitterionic PE and the pH-induced polymorphism in anionic PS. The phase behavior of DMPS in the presence of added electrolyte was also investigated by the inclusion of the screened electrostatic interactions [33] to a phenomenological model for neutral lipids [34]. Hence, the anionic-lipid aggregates may vary surface charge, geometrical form, or size in response to physical parameters (like temperature or pressure) or to changes of the solvent chemical composition, either by varying pH [29,35–39] or ionic strength [25,40–56]. Although there are some atomistic simulations treating PSs [57] and PGs [58], these works focused mainly on local interfacial properties and do not address directly the question of phase transitions induced by physicochemical variations.

Motivated by these open questions, we propose a statistical model to account for the gel-fluid anomalous phase transitions in charged lipid lamellar phases. Apart from the competition between hydrophobic energy and chain entropy, which drives the usual gel-fluid transition, in the case of dissociating lipids additional ion-mediated mechanisms, such as ionic screening and counterion association to the lipid headgroups, are expected to play an important role in determining the system properties. Although no Na$^+$ binding to anionic phospholipids in aqueous suspensions was assumed in earlier work [27,35,38], considerable evidence for measurable counterion association (more specifically, of the sodium ion Na$^+$, commonly used in experiments) to hydrated anionic phospholipid *headgroups*, including PA$^-$, PS$^-$, and PG$^-$, has been supported from theoretical interpretation of experimental measurements obtained by several independent techniques [25,37,40–56], as well as from analysis of atomistic simulations [57,58]. Such evidence motivated us to propose a generalization of the two-state statistical model for neutral lipid membranes [59–66], in which the lipid chains can be in two possible states: the (low-temperature or high-lateral-pressure) gel state or the (high-temperature or low-lateral-pressure) fluid state, through the inclusion of the effect of counterion association to the lipid headgroups, which are allowed to be in two charged states: charged (counterion dissociated, with the counterion released to the aqueous solution) or neutral (counterion associated).

It is interesting to note that early theoretical work on this subject [29] already pointed out the major role of the discrete nature of the surface charges on thermodynamic properties of ionic-lipid membranes. Later, the competitive adsorption of monovalent and divalent cations to anionic phospholipid membranes was considered as a monomer-dimer problem on

a lattice [67], but without taking the lipid-acyl chains into account. In our approach, competition between the effective van der Waals attractions of the acyl chains and the Coulomb electrostatic repulsion of charged headgroups is introduced, leading to new thermotropic behavior. As we show, the coupling between acyl-chain conformation and headgroup-charge degrees of freedom introduces new thermodynamic phases, in which headgroup charges may be spatially ordered, depending on the physicochemical parameters. Checkerboard-like ordering of charged and neutral lipids gives rise to *semidissociated* phases, in which dissociated lipid headgroups form a regular pattern on the membrane surface. Later, we will refer to this type of order as *charge order* [68].

The outline of the remainder of this work is as follows. Section II introduces the statistical model in terms of effective physical parameters. Section III presents the ground state of the model obtained directly from a zero-temperature analysis of the effective model Hamiltonian. Section IV contains a mean-field analysis of the system. Section V displays and discusses numerical results of the mean-field equations at finite temperatures. Section VI presents some concluding remarks. Appendices A and B present, respectively, the derivation of the mean-field equations by using a Gaussian transformation and by a Dirac-δ-function representation of the sublattice averages. In Appendix C the zero-temperature limit analysis of the mean-field equations is presented.

II. DEFINITION OF THE STATISTICAL MODEL

Let us consider a planar lattice of coordination number γ (e.g., $\gamma = 4$ for the square lattice) to represent one of the leaflets of an ionic dissociating lipid bilayer. The lattice contains $2N$ particles, which represent the lipid molecules. Each lipid molecule, denoted by $i = 1, \ldots, 2N$, is characterized by its acyl-chain and its headgroup states, as presented in Fig. 1. We consider two possible states for the acyl chains [$s_i = 1$, gel (low temperature or high lateral pressure) with energy ϵ_G, and $s_i = 0$, fluid (high temperature or low lateral pressure) with energy $\epsilon_F > \epsilon_G$] and two states for the ionizable lipid headgroups [$\tau_i = 0$, neutral (counterion associated, i.e., counterion bound), and $\tau_i = 1$, charged (counterion dissociated, i.e., counterion detached)]. It is assumed, therefore, that the ionic lipid headgroups contain counterion-adsorbing species [69], while coion adsorption is neglected, due to the strong electrostatic repulsion between the charged headgroup and the like-charged coion. The fluid states are multiply degenerate, the degeneracy ω corresponding to the high entropy of the disordered hydrocarbon chains of a single lipid particle. Lipid acyl chains interact via effective van der Waals (hydrophobic) interactions ϵ_{GG}, ϵ_{FF}, and ϵ_{GF} for nearest-neighbor pairs in the gel, fluid, and gel-fluid states, respectively. The effective cross-sectional areas per lipid headgroup a_F and a_G for the fluid and the gel states satisfy $a_F > a_G$, since lipids in the gel state exhibit smaller area per lipid headgroup. To the effective hydrophobic interactions we add Coulomb repulsions of electrostatic potential energy

$$V = \frac{e^2}{4\pi \varepsilon_0 \varepsilon_W d_{ij}} \equiv \frac{\tilde{V}}{d_{ij}}, \qquad (1)$$

s_i	τ_i	lipid state	schematic top view	two−letter label
1	0		○	AG: associated gel
0	0		◯	AF: associated fluid
1	1		◉	DG: dissociated gel
0	1		⊙	DF: dissociated fluid

FIG. 1. Four possible states of the lipid molecules in terms of the occupation-number variables s_i and τ_i. We also show the schematic top-view representation of the lipid headgroups, to be used later to identify the distinct thermodynamic phases: a large empty circle represents a fluid-acyl chain lipid, a small empty circle corresponds to a gel-acyl chain lipid, and an inner black circle represents a charged (counterion-dissociated or counterion-detached) lipid headgroup. Counterion association leading to a neutral lipid headgroup is represented by absence of the inner black circle. The last column displays the two-letter labels that characterize these pure states, which will be used to identify the associated homogeneous ground-state phases, cf. Table I and Figs. 2 and 4.

for nearest-neighbor pairs (i,j) of counterion-dissociated lipid headgroups, dependent on their distance d_{ij}, where e is the electronic charge, ε_0 is the permittivity of the vacuum, and ε_W is the water dielectric constant. The distance d_{ij} between particles is taken as $d_{GG} = \sqrt{a_G}$, $d_{FF} = \sqrt{a_F}$, or $d_{GF} = \frac{\sqrt{a_G}+\sqrt{a_F}}{2}$ for pairs in the gel, fluid, or gel-fluid states, accordingly. By assuming this unscreened form of the electrostatic interaction energy, we do not address the question of possible effects due to the screening by free mobile ions or due to the dielectric contrast at the interface between the aqueous medium and the acyl-chain region [70–72]. These effects become important for weakly charged interfaces and higher salt concentrations. The electrostatic strength $\tilde{V} = e^2/4\pi\varepsilon_0\varepsilon_W$ also includes other ion-dependent contributions such as ion hydration [73] and the ionic interaction with the water structured differently at the water-lipid interface. Hence, it should also be considered an effective parameter, analogously to the van der Waals energies ϵ_{ij}. Thus the model Hamiltonian is given by

$$\mathcal{H} = -\sum_{(i,j)} s_i s_j \left(\epsilon_{GG} - \tau_i \tau_j \frac{\tilde{V}}{d_{GG}} \right) - \sum_{(i,j)} (1-s_i)(1-s_j)$$
$$\times \left(\epsilon_{FF} - \tau_i \tau_j \frac{\tilde{V}}{d_{FF}} \right) - \sum_{(i,j)} [s_i(1-s_j) + (1-s_i)s_j]$$
$$\times \left(\epsilon_{GF} - \tau_i \tau_j \frac{\tilde{V}}{d_{GF}} \right) + \sum_i [s_i \epsilon_G + (1-s_i)\epsilon_F], \quad (2)$$

where i and j label lattice sites and the sums (i,j) apply to all distinct nearest-neighbor pairs of lipids. The electrostatic

interaction $\tilde{V}/d_{ij}$ is present only for pairs of nearest-neighbor charged lipids (i,j). Therefore, our model treats the electrostatic interaction as short-ranged, which might be justified only at high screening. One may question whether the spatially ordered semidissociated phases, to be presented later, would remain with the inclusion of further-neighbor interactions. Studies on models with interactions of longer range indicate that this would be indeed the case. If we consider just the charge-charge interactions, the model system may be mapped onto a lattice gas [74] with repulsive long-range interactions. This is equivalent to a long-range antiferromagnetic Ising model. Studies of the phase diagrams and critical behavior of the square-lattice antiferromagnetic Ising model with interactions between second and third neighbors, besides nearest ones [75], show that, besides the simple checkerboard antiferromagnetic phase, distinct spatially ordered phases of different geometries may also be present, depending on relative interaction strengths. Furthermore, more recently, Tröster [76] considered long-range antiferromagnetic interactions on the lattice and inferred that the critical behavior of the square-lattice antiferromagnetic Ising model with true long-range $1/r$ interactions belongs to the same universality class of the short-range Ising model. We believe, thus, that interactions of longer range should not necessarily destroy the ordered phases predicted by the short-ranged model.

In order to obtain equilibrium properties, the system free energy is more easily obtained in an ensemble of constant lateral pressure Π and fixed chemical potential of counterions μ_c, which is related to the macroscopic salt concentration, membrane surface charge, charged-lipid density, temperature, and, possibly, specific counterion-lipid interactions. Thus the associated partition function $\Xi_{2N}(T,\Pi,\mu_c)$ reads

$$\Xi_{2N}(T,\Pi,\mu_c) = \sum_{\{s_i\},\{\tau_i\}} \omega^{N_F} \exp[-\beta(\mathcal{H} + \Pi A - \mu_c N_b)]$$
$$= \sum_{\{s_i\},\{\tau_i\}} e^{-\beta\mathcal{H}_{\text{eff}}}, \quad (3)$$

with $\beta \equiv 1/(k_B T)$ and $\sum_{\{s_i\},\{\tau_i\}}$ denotes a trace over all possible 4^{2N} lipid-state configurations. The total number N_F of acyl chains in the fluid state, the total area A of the system and the total number N_b of counterion-bound (associated or neutral) lipids are given by

$$N_F = \sum_{i=1}^{2N} (1-s_i),$$
$$A = \sum_{i=1}^{2N} [a_G s_i + a_F(1-s_i)], \quad (4)$$
$$N_b = \sum_{i=1}^{2N} (1-\tau_i).$$

Note that the number of charged lipids—or the number of free counterions desorbed from the membrane and released to the aqueous solution—is dependent on the system lipid-state configuration and given by $2N - N_b$. The less counterions are associated at the lipid membrane, the larger the amount of remaining ionized headgroups and the net surface charge of the membrane.

The effective Hamiltonian $\mathcal{H}_{\text{eff}}$ in the $(T, \Pi, 2N, \mu_{\text{c}})$ ensemble may be written in simplified form as

$$\beta\mathcal{H}_{\text{eff}} = 2N\beta\varphi_0(t) - \frac{4}{\gamma t}\sum_{(i,j)} s_i s_j + \frac{\upsilon}{\gamma t}\sum_{(i,j)} \tau_i \tau_j [1 + \lambda_1 s_i s_j$$
$$+ \lambda_2(s_i + s_j)] + \frac{h(t)}{t}\sum_i s_i + \frac{\mu}{t}\sum_i \tau_i, \qquad (5)$$

with the new parameters defined by

$$\varphi_0(t) \equiv -\mu_{\text{c}} + \epsilon_{\text{F}} - \frac{\gamma\epsilon_{\text{FF}}}{2} + \Pi a_{\text{F}} - Jt\ln\omega,$$

$$J \equiv \frac{\gamma}{4}(\epsilon_{\text{GG}} + \epsilon_{\text{FF}} - 2\epsilon_{\text{GF}}) > 0, \quad t \equiv \frac{k_{\text{B}}T}{J} > 0,$$

$$\upsilon \equiv \frac{\gamma\tilde{V}}{Jd_{\text{FF}}} > 0, \quad \lambda_1 \equiv \frac{(\lambda-1)^2}{\lambda+1} > 0,$$

$$\lambda_2 \equiv \frac{\lambda-1}{\lambda+1} > 0, \quad p \equiv \frac{2\Pi\Delta a + \Delta\epsilon}{4J},$$

$$h(t) \equiv 2 + t\ln\omega - 2p, \quad \mu \equiv \frac{\mu_{\text{c}}}{J}, \qquad (6)$$

in which $\lambda \equiv d_{\text{FF}}/d_{\text{GG}} > 1$, $\Delta a = a_{\text{F}} - a_{\text{G}} > 0$, $\Delta\epsilon = 2(\epsilon_{\text{F}} - \epsilon_{\text{G}}) + \gamma(\epsilon_{\text{GG}} - \epsilon_{\text{FF}}) > 0$. This effective Hamiltonian can be mapped onto an Ashkin-Teller model [77] with the inclusion of cubic terms [78], but we will perform the calculations using occupation-number (s, τ) variables, since the correspondence and comparison between the models have little usefulness. The ferromagnetic condition on the nearest-neighbor coupling of the $\{s_i\}$ variables, $J > 0$, expresses the fact that gel and fluid lipids tend to demix, leading to phase separation at coexistence conditions. The neutral version of our model can be mapped onto the Ising ferromagnet. Note that full association leading to a neutral system can be achieved by setting the limit $\mu \to \infty$ in our model, or, equivalently, $\tau_i = 0$. Then, if occupation-number variables $s_i = 0, 1$ are replaced by symmetric variables $(2s_i - 1) = \pm 1$ in the effective Hamiltonian (5), one may note that the first-order transition at finite temperatures takes
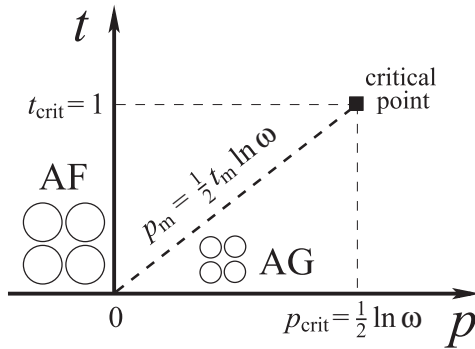

FIG. 2. Mean-field phase diagram of the model system in the $\mu \to \infty$ limit (strong ionic screening), which can be mapped onto the standard Ising model in a uniform magnetic field. The melting first-order dashed line at lower temperatures $t < 1$ ($h_{\text{m}} = 2 \leftrightarrow p_{\text{m}} = \frac{1}{2}t_{\text{m}}\ln\omega$) separating the AF and AG phases terminates at the critical point (black square) $p_{\text{crit}} = \frac{1}{2}\ln\omega$, $t_{\text{crit}} = 1$. The critical order parameters are $m_{\text{crit}} = \frac{1}{2}$ and $\alpha_{\text{crit}} = q_{\text{crit}} = 0$. Close to the two-letter labels of the uncharged AF and AG phases, we show their associated lattice configuration using the schematic top-view representation of the lipid headgroups introduced in Fig. 1.

place at the melting line $h_{\text{m}} = 2$ (or $2p_{\text{m}} = t_{\text{m}}\ln\omega$), as shown in Fig. 2, corresponding to the vanishing uniform external magnetic field of the associated Ising model [59,79]. For the standard ferromagnetic Ising model, there are no *thermotropic* first-order phase transitions. Here, however, these are possible due to the high degeneracy $\omega \gg 1$ of the fluid acyl-chain states.

One should also mention that inclusion of repulsive $(J_2 < 0)$ next-nearest-neighbor interactions $-J_2 \sum_{(i,k)} s_i s_k$ along a fixed direction in the model Hamiltonian may account for the so-called pretransition [22] and its associated rippled phase [80], observed experimentally in zwitterionic or ionic lipid suspensions.

III. THE GROUND STATE

The ground state of the model may be obtained by analysis of the zero-temperature limit of the effective Hamiltonian, Eq. (5), while finite-temperature properties are obtained, later in this work, within a mean-field framework assuming a two-sublattice division of the system, as shown in Fig. 3. To obtain the correct ordered phases at lower temperatures it is crucial to consider this subdivision.

For the neutral membrane model, the system presents only two thermodynamic states at $T = 0$, the gel (G) and the fluid (F) states, which coexist at the lateral pressure $\Pi_{\text{m}} = -\Delta\epsilon/2\Delta a$ corresponding to $p_{\text{m}} = 0$, cf. Eq. (6). For ionic dissociating lipids, at a first look, one may expect the appearance of four phases, correspondingly dissociated gel (DG) and dissociated fluid (DF) phases, as well as two associated phases, an associated gel (AG) and an associated fluid (AF) phase, the latter two reducing to the G and F states of the neutral system in the $\mu \to \infty$ limit. However, the competition that arises between the tendency to dissociate, which decreases as salt is added (or as μ_{c} rises), and the drive to associate, in order to lower the system electrostatic energy, yields two other possibilities: semidissociated gel (SG) and semidissociated fluid (SF) phases, in which all headgroups in one of the sublattices are ionized (counterion-dissociated), whereas in the other they are associated (neutralized by adsorbed counterions). Henceforth, we refer to this type of checkerboard-like order as *charge order*. The existence of such charge-ordered phases can be understood in terms of the effective Hamiltonian, Eq. (5). By mapping it onto an Ashkin-Teller model, the effective coupling between the $\{\tau_i\}$ variables is antiferromagnetic-like, implying a spatially ordered ground state for low temperatures and weak effective magnetic fields
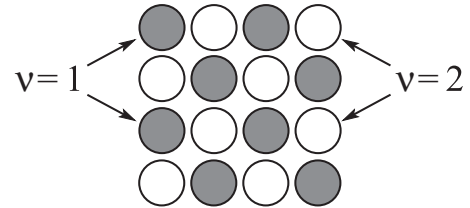

FIG. 3. Subdivision of a square lattice in two interpenetrating sublattices, labeled by $\nu = 1$ (shaded sites) and $\nu = 2$ (unshaded sites). Assuming only nearest-neighbor interactions, a site in the $\nu = 1$ sublattice interacts only with sites in the $\nu = 2$ complementary sublattice.

TABLE I. Ground-state phases obtained by analysis of the effective Hamiltonian Eq. (5) at $T = 0$. $\Delta \psi_0 \equiv \mathcal{H}_{\text{eff}}/2N - \varphi_0(t=0)$ represents the ground-state free energy per lipid. In the semidissociated (SF and SG) phases, the sites i and j that define a nearest-neighbor pair (i,j) belong, each one, to two distinct interpenetrating sublattices, as shown in Fig. 3. The two different τ values for the SF and SG phases are associated with each one of these two distinct sublattices.

Phase	s	τ	$\Delta\psi_0/J$
AF	0	0	0
AG	1	0	$-2p$
DF	0	1	$\mu + \upsilon/2$
DG	1	1	$-2p + \mu + \lambda\upsilon/2$
SF	0	1,0	$\mu/2$
SG	1	1,0	$-2p + \mu/2$

[81]. In terms of the original occupation-number representation, the ordered staggered states are associated with the aforementioned semidissociated phases. Therefore, to obtain these two latter phases, it is crucial to consider a two-sublattice division of the system—each containing N particles—in order to compute the nearest-neighbor sums (i,j) of the effective Hamiltonian, Eq. (5). We also explore the possibility of occurrence of a staggered phase in the $\{s_i\}$ variables, but for the set of parameters chosen, this type of ordering is always associated with higher free energies.

The possible ground-state phases and respective effective free energies per lipid are listed in Table I.

Taking into account the phases proposed in Table I, the ground-state transitions can be determined and are given in Table II.

Thus new charge-ordered (semidissociated) phases emerge from the study of the ground state under different ionic strengths. Collecting all information derived directly from the effective Hamiltonian, given by Table II, as well as from the zero-temperature limit of the mean-field equations from the Appendix C, yields the ground-state phase diagram depicted in Fig. 4, which displays the $T = 0$ possible phases in the $\mu \times p$ plane. The role of the counterion chemical potential μ is to neutralize the membrane charge at higher values, when the counterions stay associated (AG and AF) with the ionizable lipid headgroups on the membrane, forming a neutral complex that reduces the surface charge density. As in the neutral membrane, for $\mu > 0$ the ordered-chain phase is present at higher lateral pressure ($p > 0$), and chains melt at lower pressure ($p < 0$), even at zero temperature, regardless of salt concentration. At intermediate values of μ ($-\upsilon < \mu < 0$, $-4p - \upsilon < \mu < 0$, or $-\lambda\upsilon < \mu < 0$, depending on p; see Fig. 4), at which the counterions tend to

TABLE II. Ground-state transitions at $T = 0$ obtained by comparing the free energies of Table I.

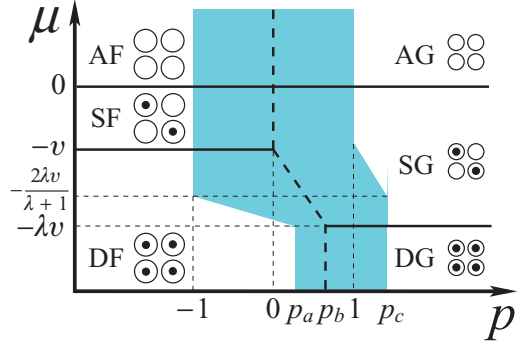| Phases	AG	SF	DG	DF
AF	$p = 0$	$\mu = 0$	—	—
SG	$\mu = 0$	$p = 0$	$\mu = -\lambda\upsilon$	$\mu = -4p - \upsilon$
DF	—	$\mu = -\upsilon$	$p = (\lambda-1)\upsilon/4$	—

FIG. 4. (Color online) Phase structures in the ground state ($t = 0$) of the model system. The thick lines represent the transitions derived directly from the effective Hamiltonian, listed in Table II. At finite temperatures the solid lines become critical (associated to continuous second-order transitions) while the dashed lines preserve their discontinuous character (related to first-order transitions), at least for lower temperatures. In the shaded regions around the first-order lines one of the coexistent phases is metastable, as derived in Appendix C from the zero-temperature limit of the mean-field equations. The parameter values marked on the axes are $p_a = -1 + (\frac{\lambda-1}{\lambda+1})\frac{\lambda\upsilon}{2}$, $p_b = (\lambda - 1)\frac{\upsilon}{4}$, $p_c = 1 + (\frac{\lambda-1}{\lambda+1})\frac{\upsilon}{2}$. The pictures close to the two-letter identification of the distinct phases represent their associated top-view configuration of the lipid headgroups, as introduced in Fig. 1.

dissociate from the lipid membrane, ionization competes with chain ordering through the repulsive electrostatic interactions between charged headgroups, and semidissociated phases (SG and SF) arise. At still lower chemical potentials ($\mu < -\upsilon$, $\mu < -4p - \upsilon$ or $\mu < -\lambda\upsilon$, depending on p; see Fig. 4) the dissociation tendency wins over the electrostatic interaction, and dissociated phases (DG and DF) arise. In the latter case, the ionized ordered phase loses stability at higher pressures, as compared to the fully associated (neutral) membrane. Note also that the width of the μ range where a charge-ordered phase exists is proportional to the dimensionless parameter υ for the fluid SF phase, and between υ and $\lambda\upsilon$ for the gel SG phase, as shown in the ground-state phase diagram of Fig. 4.

The discussion of the system ground state presented in the previous paragraphs was based on the $(T, \Pi, 2N, \mu_c)$ ensemble calculations, which was chosen for mathematical convenience. In relation to charge density on the bilayer surface, this ensemble corresponds to a *grand-canonical ensemble for the counterions* adsorbed to the membrane plane. The electrolytic solvent is represented by a bath of constant chemical potential for counterions μ_c. Thus adsorption of counterions on the membrane surface is regulated by the counterion chemical potential, as for a lattice gas [74], and, correspondingly, a very low (or negative) chemical potential implies very low counterion density and a highly charged surface, while the opposite case is reached at very high (positive) chemical potential, which yields a scarcely charged surface.

But what values for chemical potential are to be expected for the lipid dispersion? To obtain the explicit dependence of μ on directly measured experimental parameters (like temperature, lipid concentration and ionic strength), one should treat the charged membrane surface and the counterion distribution in the electrolytic solution self consistently, which is a subject of future work. However, some interpretation in terms of

arguments on counterion condensation may be anticipated. Even though the membrane surface is treated as an infinite plane in the model we propose, our aim is to apply it also to the case of unilamellar vesicles (spherical geometry). In this respect, one may rely on some general results for counterion condensation at $T = 0$, which depend on the membrane geometry [82]. In the case of planar symmetry, complete counterion condensation should take place at $T = 0$, which implies a neutral membrane. According to Fig. 4, the ground-state chemical potential should remain strictly positive, $\mu(T = 0) > 0$, and the lower part of the phase diagram would lose physical meaning. However, for spherical symmetry in the strong dilution regime of charged lipids, full condensation may not occur at $T = 0$, making possible, according to Fig. 4, a negative ground-state chemical potential, $\mu(T = 0) < 0$. Thus our results for a charged membrane at $T = 0$ in the $\mu < 0$ region may be given an interpretation in terms of the electrolytic distribution of counterions on spherical symmetry.

IV. MEAN-FIELD EQUATIONS

A. Sublattice averages, order parameters and conjugated fields

In our further study for $T \neq 0$, model equilibrium properties are obtained under a Curie-Weiss mean-field approach [83], in which interactions are taken as long ranged and independent of distance. The study of the ground state performed in Sec. III, which indicates the existence of the semidissociated phases, points to the necessity of subdivision of the system into two identical interpenetrating sublattices, each containing N sites, to be represented as $\nu = 1,2$, as depicted in Fig. 3. To allow an exact evaluation of Eq. (3), the sums over nearest-neighbor pairs (i,j) in Eq. (5) are replaced by

$$\sum_{(i,j)} \sigma_i \sigma_j \rightarrow \frac{\gamma}{N} \left(\sum_{\substack{i=1 \\ i \in \nu}}^{N} \sigma_i \right) \left(\sum_{\substack{j=1 \\ j \in \bar{\nu}}}^{N} \sigma_j \right), \quad (7)$$

for $\sigma = s$, τ, or $s\tau$. The prefactor γ/N is introduced in order to ensure a proper and well-defined thermodynamic limit $N \rightarrow \infty$ [84] and also preserves the ground state of the original system with short-range interactions. The symbol $\bar{\nu}$ labels the sublattice complementary to ν, e.g., if $\nu = 1$ then $\bar{\nu} = 2$ and vice versa. For this reason, one must also introduce the sublattice averages for chain states, counterion-dissociation states, and the corresponding couplings,

$$m_\nu \equiv \langle s \rangle_\nu = \frac{1}{N} \sum_{\substack{i=1 \\ i \in \nu}}^{N} s_i,$$

$$\alpha_\nu \equiv \langle \tau \rangle_\nu = \frac{1}{N} \sum_{\substack{i=1 \\ i \in \nu}}^{N} \tau_i, \quad (8)$$

$$q_\nu \equiv \langle s\tau \rangle_\nu = \frac{1}{N} \sum_{\substack{i=1 \\ i \in \nu}}^{N} s_i \tau_i.$$

To characterize the different ordered phases, it is convenient to define the uniform thermodynamic order parameters,

$$m \equiv \tfrac{1}{2}(m_1 + m_2), \quad \alpha \equiv \tfrac{1}{2}(\alpha_1 + \alpha_2), \quad q \equiv \tfrac{1}{2}(q_1 + q_2), \quad (9)$$

as well as the staggered thermodynamic order parameters,

$$m^\dagger \equiv \tfrac{1}{2}(m_1 - m_2), \quad \alpha^\dagger \equiv \tfrac{1}{2}(\alpha_1 - \alpha_2), \quad q^\dagger \equiv \tfrac{1}{2}(q_1 - q_2). \quad (10)$$

Nonvanishing staggered order parameters represent semidissociated (charge-ordered) phases, while homogeneous (charge-disordered) phases have always $m^\dagger = \alpha^\dagger = q^\dagger = 0$. The acyl-chain order parameter m corresponds to the fraction of lipids in the gel phase ($m = 0$: completely disordered, fluid phase; $m = 1$: completely ordered, gel phase), while the charge order parameter α (degree of ionization) gives the fraction of ionized lipid headgroups ($\alpha = 0$: fully associated neutral phase; $\alpha = 1$: fully dissociated charged phase).

Furthermore, in order to calculate the above-defined sublattice averages $(m_\nu, \alpha_\nu, q_\nu)$, conjugated sublattice virtual fields Π_ν, μ_ν^c, and Θ_ν need to be introduced into the model Hamiltonian, so the contribution $\Pi A - \mu_c N_b$ to Eq. (5) is replaced by

$$\sum_{\nu=1,2} \Pi_\nu \sum_{\substack{i=1 \\ i \in \nu}}^{N} [a_{\mathrm{G}} s_i + a_{\mathrm{F}}(1 - s_i)] - \sum_{\nu=1,2} \mu_\nu^c \sum_{\substack{i=1 \\ i \in \nu}}^{N} (1 - \tau_i)$$

$$- \sum_{\nu=1,2} \Theta_\nu \sum_{\substack{i=1 \\ i \in \nu}}^{N} s_i \tau_i. \quad (11)$$

At the end of the calculations we take $\Pi_1 = \Pi_2 = \Pi$, $\mu_1^c = \mu_2^c = \mu_c$, $\Theta_1 = \Theta_2 = 0$. Besides the homogeneous parameters, Eqs. (6), for mathematical convenience we introduce the dimensionless conjugate fields associated with each sublattice,

$$p_\nu \equiv \frac{2\Pi_\nu \Delta a + \Delta \epsilon}{4J}, \quad h_\nu(t) \equiv 2 + t \ln \omega - 2p_\nu,$$

$$\mu_\nu \equiv \frac{\mu_\nu^c}{J}, \quad \theta_\nu \equiv \frac{\Theta_\nu}{J}. \quad (12)$$

In terms of these conjugate virtual fields, the effective two-sublattice Hamiltonian, from Eq. (5), then reads

$$\beta \mathcal{H}_{\mathrm{eff}} = 2N\beta\varphi_0(t) - \frac{4}{\gamma t} \sum_{(i \in \nu,\, j \in \bar{\nu})} s_i s_j$$

$$+ \frac{\upsilon}{\gamma t} \sum_{(i \in \nu,\, j \in \bar{\nu})} \tau_i \tau_j [1 + \lambda_1 s_i s_j + \lambda_2 (s_i + s_j)]$$

$$+ \frac{1}{t} \sum_{\nu=1,2} \sum_{\substack{i=1 \\ i \in \nu}}^{N} [h_\nu(t) s_i + \mu_\nu \tau_i - \theta_\nu s_i \tau_i]. \quad (13)$$

B. Mean-field free-energy functional

To proceed with the calculations, we express the effective Hamiltonian Eq. (13) as a density per lipid particle, in terms of the sublattice averages, Eqs. (8),

$$\frac{1}{2N}\mathcal{H}_{\text{eff}} = \varphi_0(t) + \varphi_1 + \varphi_2, \qquad (14)$$

$$\beta\varphi_1 = \frac{1}{2t}\sum_{\nu=1,2}(h_\nu m_\nu + \mu_\nu \alpha_\nu - \theta_\nu q_\nu), \qquad (15)$$

$$\beta\varphi_2 = -\frac{2}{t}m_1 m_2 + \frac{\upsilon}{2t}[\alpha_1\alpha_2 + \lambda_1 q_1 q_2 + \lambda_2(\alpha_1 q_2 + \alpha_2 q_1)], \qquad (16)$$

in which φ_1 and φ_2 correspond to linear and quadratic contributions.

After diagonalization of the quadratic terms of φ_2, one may use the Gaussian transformation

$$e^{\pm k\eta^2} = \sqrt{k/\pi}\int_{-\infty}^{\infty}dx\, e^{-kx^2 + 2\eta kx\sqrt{\pm 1}}, \qquad (17)$$

in order to linearize the Hamiltonian in the particle-state variables. An exact summation of Eq. (3) may be then performed, leading to a free-energy functional $\Psi_{2N}(T,\Pi,\mu_c;\boldsymbol{r})$ in terms of a six-dimensional auxiliary continuous field $\boldsymbol{r} \equiv (x,y,z,x^\dagger,y^\dagger,z^\dagger)$. The integration over $\boldsymbol{r}$ is performed by using the steepest-descent method. Equations of state connect thermodynamic order parameters and the stationary points $\bar{\boldsymbol{r}}$ of the free-energy functional Ψ_{2N}, whose extremum [85] corresponds to the extensive thermodynamic free energy

$$\psi_{2N}(T,\Pi,\mu_c) \equiv -k_B T \ln \Xi_{2N} = \Psi_{2N}(T,\Pi,\mu_c;\boldsymbol{r}=\bar{\boldsymbol{r}})$$
$$= \underset{\boldsymbol{r}}{\text{extr}}\,\Psi_{2N}(T,\Pi,\mu_c;\boldsymbol{r}). \qquad (18)$$

After extremization of the functional $\Psi_{2N}(T,\Pi,\mu_c;\boldsymbol{r})$, we obtain, in the thermodynamic limit $N \to \infty$, the mean-field free energy per lipid

$$\psi(T,\Pi,\mu_c) = \lim_{N\to\infty}\frac{1}{2N}\psi_{2N}(T,\Pi,\mu_c), \qquad (19)$$

leading to Eq. (25) of the next subsection. Further details of the calculations are given in Appendix A. In Appendix B we present an alternative derivation of the mean-field equations based on a Dirac-δ-function representation of the sublattice averages (m_ν,α_ν,q_ν).

C. Mean-field equations of state and free energy

The thermodynamic free energy of the system per lipid $\psi(T,\Pi,\mu_c)$ is obtained from the stationary-point conditions of the free-energy functional $\nabla\Psi(\boldsymbol{r}=\bar{\boldsymbol{r}}) = \boldsymbol{0}$ for the six-dimensional stationary points $\bar{\boldsymbol{r}} \equiv (\bar{x},\bar{y},\bar{z},\bar{x}^\dagger,\bar{y}^\dagger,\bar{z}^\dagger)$, leading to Eqs. (A15) of Appendix A. These relations yield the following mean-field equations of state for the thermal self-averages of sublattice $\nu=1$,

$$m_1 \equiv \langle s\rangle_1 = \frac{e^{\beta\phi_{10}^{(1)}} + e^{\beta\phi_{11}^{(1)}}}{\xi_1}, \quad \alpha_1 \equiv \langle \tau\rangle_1 = \frac{e^{\beta\phi_{01}^{(1)}} + e^{\beta\phi_{11}^{(1)}}}{\xi_1},$$
$$q_1 \equiv \langle s\tau\rangle_1 = \frac{e^{\beta\phi_{11}^{(1)}}}{\xi_1}, \qquad (20)$$

in terms of the single-site effective partition function of sublattice $\nu=1$,

$$\xi_1 \equiv \sum_{s,\tau\in\nu=1} e^{\beta\phi_{s\tau}^{(1)}}, \qquad (21)$$

and the effective fields $\phi_{s\tau}^{(1)}$ (with $\phi_{00}^{(1)} \equiv 0$),

$$\beta\phi_{10}^{(1)} = \frac{2p}{t} + \frac{2(2m_2 - 1)}{t} - \ln\omega, \qquad (22)$$

$$\beta\phi_{01}^{(1)} = -\frac{\mu}{t} - \frac{\upsilon}{t}\left(\alpha_2 + \frac{\lambda - 1}{\lambda + 1}q_2\right), \qquad (23)$$

$$\beta\phi_{11}^{(1)} = \beta\phi_{10}^{(1)} - \frac{\mu}{t} - \frac{\upsilon}{t}\left[\frac{2\lambda}{\lambda+1}\alpha_2 + \frac{\lambda(\lambda-1)}{\lambda+1}q_2\right]. \quad (24)$$

The equations of state for the thermal self-averages of sublattice $\nu=2$ are obtained switching the sublattice labels $1 \to 2$ and $2 \to 1$ in Eqs. (20)–(24). Therefore, the leading term of the homogeneous ground-state phase corresponding to $(s = m_1 = m_2 = m, \tau = \alpha_1 = \alpha_2 = \alpha)$ is given by $e^{\beta\phi_{m\alpha}}$.

Replacing the stationary points $\bar{\boldsymbol{r}}$, Eqs. (A15), into the mean-field free-energy functional, Eq. (A13), one obtains the appropriate thermodynamic free energy per lipid [86] $\psi = \Psi(\boldsymbol{r} = \bar{\boldsymbol{r}})$,

$$\beta\psi = \beta\varphi_0(t) + \frac{2}{t}m_1 m_2 - \frac{\upsilon}{2t}\left[\alpha_1\alpha_2 + \frac{(\lambda-1)^2}{\lambda+1}q_1 q_2\right.$$
$$\left. + \frac{\lambda-1}{\lambda+1}(\alpha_1 q_2 + \alpha_2 q_1)\right] - \frac{1}{2}\sum_{\nu=1,2}\ln\xi_\nu. \qquad (25)$$

In the zero-temperature limit, it reduces to the mean-field ground-state free energy per lipid $\psi_0 \equiv \psi(T=0) = \mathcal{H}_{\text{eff}}(T=0)/2N$,

$$\psi_0(m_1,m_2;\alpha_1,\alpha_2;q_1,q_2) = \varphi_0(t=0) + 2Jm_1 m_2$$
$$- \frac{J\upsilon}{2}\left[\alpha_1\alpha_2 + \frac{(\lambda-1)^2}{\lambda+1}q_1 q_2 + \frac{\lambda-1}{\lambda+1}(\alpha_1 q_2 + \alpha_2 q_1)\right]$$
$$- \frac{1}{2}\sum_{\nu=1,2}\max\left(0,\phi_{10}^{(\nu)},\phi_{01}^{(\nu)},\phi_{11}^{(\nu)}\right). \qquad (26)$$

This mean-field expression for the ground-state free energy leads to exactly the same results given in Tables I and II from analysis of the original Hamiltonian, Eq. (5), since parameters used in the transformation of the sums over nearest-neighbor pairs (i,j), given by Eqs. (7), were performed such as to yield the same ground state of the system with short-range interactions.

V. NUMERICAL ANALYSIS AND DISCUSSION OF THE MEAN-FIELD EQUATIONS

In order to probe the general thermodynamic properties of the model, in this work we investigate its behavior in terms of arbitrary model parameters in an initial exploratory study. For concreteness, below we define the values of parameters that will be used hereafter in order to perform the numerical calculations. Although we consider the model on a square lattice of coordination $\gamma = 4$, its value is already incorporated into the definition of the dimensionless variables, cf. Eqs. (6). The value for $\lambda = 1.3$ was based on model parameter estimates of the area per lipid headgroup for the gel $a_G \approx 40.8$ Å^2 and

fluid states $a_F \approx 68$ Å^2 for two acyl chains with 16 carbons [61]. The disordered single-chain degeneracy ω was chosen large and set to $\omega = 3.5 \times 10^5$, also based on estimates for acyl chains with 16 carbons [61]. We have investigated the model behavior under conditions for which the gel phase is present at lower temperatures, which implies fixing lateral pressure at higher values, as can be seen from Fig. 4 for the ground-state phase diagram, $p > p_b = (\lambda - 1)\upsilon/4$. As there are no direct and accurate experimental measurements for the parameters p [87] and υ for bilayered vesicles, we arbitrarily set $p = 0.15$ (chosen in order to always satisfy $p > p_b$) while the parameter υ was varied in order to investigate the role of the electrostatic interactions.

Our interest lies in investigating the thermal and electrical properties of the model under different ionic-strength conditions. In our approach, salt concentration is represented through the chemical potential of counterions μ_c, with high salt concentration associated with larger values for μ_c. We have looked at the effect of varying salt concentration and at the importance of the Coulomb interaction with respect to the phases displayed by the system at different temperatures. Finally, we consider the thermodynamic behavior of some experimentally relevant quantities, like the specific heat and degree of ionization (fraction of charged lipid headgroups). These theoretical results already show the most important emergent feature of the model, namely the possibility of charge-ordered phases and their possible connection with the anomalous transition region [18]. In a companion paper, model results shall be compared semiquantitatively to experiments for dispersions of the ionic lipids PGs [88].

A. General properties

In order to establish the model phase diagrams, Eqs. (20) for the sublattice $\nu = 1$ averages (m_1, α_1, q_1) and similar equations for the sublattice $\nu = 2$ averages, as explained previously (Sec. IV C), must be studied numerically.

Figures 5–7 illustrate the behavior of the degree of ionization α, Eq. (9), in cases for which a semidissociated phase (SG or SF) is present in different regions of the phase diagram (dimensionless chemical potential of counterions μ versus dimensionless temperature t). Figures 5 and 6 display solutions for α at fixed temperature t and increasing μ, whereas Fig. 7 shows behavior of α at fixed μ and increasing temperature t.

Figure 5 shows two different sets of solutions for the sublattice ionizations, Eqs. (20)–(24), as obtained from the numerical study. Note that only one of the sets is thermodynamically stable, i.e., associated to lower values of the particle free energy ψ, Eq. (25). In order to distinguish between thermodynamically stable and metastable mean-field solutions, we will denote them by capital and lowercase letters, respectively. At the same time, they will be identified by solid and dot-dashed lines, respectively. For example, the label df in Fig. 5 denotes a metastable solution (dot-dashed line) associated with a DF phase. Far from the first-order transition, it may occur that there is only one solution to Eqs. (20)–(24), for example, at much higher temperatures than $t = 0.05$ of Fig. 8. In this case, this unique solution corresponds to the stable thermodynamic state of the system.
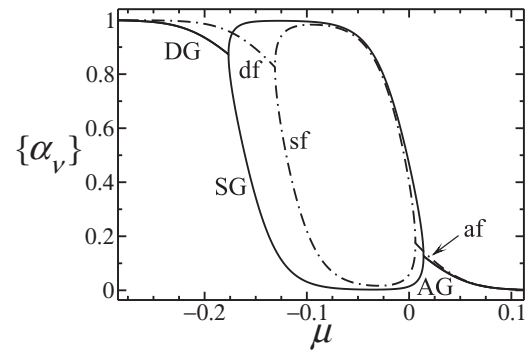
FIG. 5. Bifurcation diagram for the degree of ionization α as a function of the dimensionless chemical potential μ, obtained by numerical solution of the mean-field equations of state. Besides the standard values of parameters (λ, ω, p) given at the start of Sec. V, we set $\upsilon = 0.125$ and $t = 0.018$. Henceforth we will use capital letters to label thermodynamically stable phases (solid lines), while metastable mean-field solutions (dot-dashed lines) will be denoted by the corresponding lowercase letters. Thus, at this particular value of dimensionless temperature t, the fluidlike solutions (df, sf, and af)—whose acyl chains are mainly disordered ($m \approx 0$)—are always metastable, while the more ordered ($m \approx 1$) gel-like ones (DG, SG, and AG) remain stable; see associated phase diagram in Fig. 8. For intermediate values of μ, the solutions split into two values, corresponding to α_1 and α_2, which represent the degrees of ionization of sublattices 1 and 2, respectively.

Figure 5 illustrates the different phases found at the low temperature $t = 0.018$. The system remains in the chain ordered gel (G) phase, with $m \approx 1$ (data not shown). However, the lipid-headgroup ionization state changes as the counterion chemical potential is varied: at low ionic strength (large negative values of μ), the membrane surface is completely
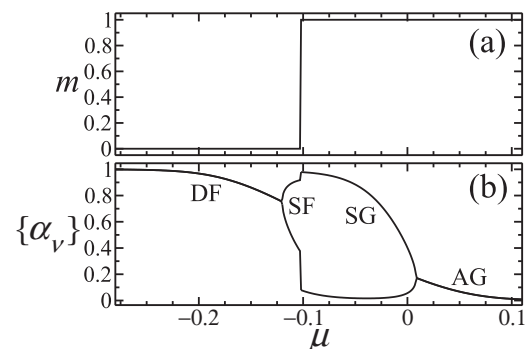
FIG. 6. Thermodynamically stable solutions for the fraction of lipids in the gel state m (a) and for the degree of ionization α (b) as a function of the dimensionless chemical potential μ. These order parameters are associated with the acyl-chain states and with the ionic polar-headgroups states, respectively. We set $\upsilon = 0.125$, $t = 0.02323$ and standard values of parameters (λ, ω, p). The order parameter m, although not visible on this scale, also splits in two very close solutions $m_1 \neq m_2$ when $\alpha^\dagger \neq 0$ (SF and SG phases), but $m_1 \approx m_2$, leading to $m^\dagger \approx 0$. The first-order transition at $\mu \approx -0.1$ is found by comparing the free energies associated with the two possible staggered solutions. The procedure is analogous to that presented in Fig. 7, in which the first-order transition dimensionless temperature $t \approx 0.023$ is found for fixed μ.

FIG. 7. Analysis of the thermodynamical stability of the mean-field solutions for the determination of the first-order transition dimensionless temperature $t_m \approx 0.023$. We set $\upsilon = 0.125$, $\mu = -0.05$ and standard values of parameters (λ, ω, p). Top portion (a) presents the two different staggered solutions characterized by their values of (α_1, α_2) and bottom part (b) shows the associated free energies differences $\Delta\psi \equiv \psi - \varphi_0(t)$ in unities of J. Although not shown, we obtain, as in Fig. 6, $m_\nu \approx 1$ for the SG, sg, and g solutions, and $m_\nu \approx 0$ for the sf, SF, and F solutions. The first-order transition takes place at the value of dimensionless temperature where the free energies of the two solutions coincide. As in Fig. 5, capital letters label thermodynamically stable phases (solid lines)—associated with lower values of ψ—while metastable mean-field solutions (dot-dashed lines) are denoted by the corresponding lowercase letters.

ionized ($\alpha_1 = \alpha_2 \approx 1$); at intermediate salt concentrations two values for α arise ($\alpha_1 \neq \alpha_2$), indicating the presence of a charge-ordered (semidissociated) phase; and, finally, at higher salt concentrations (large positive values of μ), the system remains associated, with $\alpha_1 = \alpha_2 \approx 0$.

The occurrence of multiple solutions for some thermo-dynamic density, as is the case illustrated in Fig. 5 for the charge density, indicates the possibility of coexistence between several phases, as well as first-order transitions between them. The location of the first-order transition is determined by the comparison of the free energies Eq. (25) associated with the multiple solutions. This is the situation illustrated by Fig. 6 for a higher temperature as compared to that of Fig. 5.

Figure 6 displays the thermodynamic stable solutions both for the acyl-chain order parameter m [Fig. 6(a)], which represents the fraction of lipids in the gel state, and the degree of ionization α [Fig. 6(b)], which represents the fraction of ionized lipids. As in the previous case, as the salt concentration increases, a semidissociated (S) chain disordered fluid (F) phase emerges continuously from a counterion-dissociated (D) fluid (F) phase. However, under further increase of μ, ionization α undergoes an abrupt variation accompanying the discontinuous disorder-order transition for the acyl chains, as can be seen in Fig. 6(b) (SF-SG transition). Clearly, this discontinuity in α (associated with a net counterion adsorption) is strongly coupled to a decrease of the area per lipid headgroup, from lipids in the more ionized fluid to the less charged gel states. At even higher values of μ the

FIG. 8. Typical mean-field phase diagram in the $\mu \times t$ plane for strong electrostatic interaction ($\upsilon = 0.125$) and standard values of parameters (λ, ω, p). Solid lines are critical [being associated to continuous (second-order) transitions] while dashed lines represent discontinuous (first-order) transitions. The black circles represent critical end points, where first-order lines meet at the ending of a second-order line. The two-letter regions label the different thermodynamic phases associated with the ground-state structures shown in Fig. 4. The arrows on the axes indicate the values of parameters kept fixed to perform the scans presented in Figs. 5 to 7.

semidissociated SG phase undergoes a continuous transition to a homogeneous AG phase.

Figure 7 illustrates the thermodynamic stability analysis of the different numerical solutions for the charge order parameter α. The evolution of the two different sets of solutions for (α_1, α_2) can be seen in Fig. 7(a), as temperature rises at fixed chemical potential μ. It should be noted that, even for the charge-ordered phases with $\alpha^\dagger \neq 0$, the acyl-chain staggered order parameter $m^\dagger$ (not shown) still remains very close to 0, i.e., residually ferrimagnetic for the associated magnetic model. If acyl chains are disordered [sf and SF solutions: dot-dashed lines that turn into solid ones in Fig. 7(a)], charge order disappears at lower temperatures ($t \approx 0.031$), whereas for ordered acyl chains [SG and sg solutions: solid lines that change into dot-dashed ones in Fig. 7(a)] the charge disordering transition occurs at a higher temperature ($t \approx 0.039$). Figure 7(b) shows the values of the free energy Eq. (25) for both sets of solutions of the order parameters, indicating that the charge order parameter α undergoes a discontinuous transition accompanying the main lipid-chain transition at $t \approx 0.023$ but remains charge-ordered beyond that transition and then disorders continuously at some higher temperature $t \approx 0.031$.

Thus acyl-chain disordering is followed by charge disordering as temperature is raised for fixed μ. From the mathematical point of view, the transitions from the charge-disordered (homogeneous) to the charge-ordered (semidissociated) phase at intermediate values of μ correspond to continuous bifurcations of fixed points (uniform solutions) to a period-2 limit cycle (staggered solutions) and represent ordinary second-order transitions [81]. On the other hand, at the gel-fluid transition, ionization α as well as the fraction of lipids in the gel state m vary abruptly and discontinuously. Therefore, in this latter case, we have a first-order transition.

In summary, the model displays two types of order: the fluid to gel transition corresponding to acyl-chain ordering and the "charge-ordering transitions" between semidissociated and homogeneous (either neutral counterion-associated or charged counterion-dissociated) phases. These two types of transition may be associated with the corresponding Ising models obtained through the formal mapping [see the effective Hamiltonian Eq. (5)]: a *ferromagnetic* Ising model couples the chain states, whereas an *antiferromagnetic* Ising model couples the ion lattice-gas states. Despite the cubic and quartic couplings between the two models [see, again, Eq. (5)] the *ferromagnetic* Ising interactions govern the gel-fluid first-order transition (if lateral pressure p is maintained below the critical point), while the *antiferromagnetic* Ising interactions control the critical ion-association order-disorder transition. Thus the type of the predicted transitions in the coupled model reflects the order of the transition of their associated Ising models at the decoupled level, which are either ferromagnetic (first-order transition), for chain order, or antiferromagnetic (second-order transition), for charge order.

B. Effect of varying chain lengths on the $\mu \times t$ phase diagrams

To better appreciate the role of the competition between the intralamellar interactions—effective van der Waals attractions (J) and Coulomb repulsions ($\tilde{V}$)—in determining the possible thermodynamic phases, we explore the $\mu \times t$ phase diagrams for different values of the dimensionless parameter $\upsilon \equiv \gamma \tilde{V}/J d_F$, which gives a measure of the importance of the electrostatic interactions. The mean-field approach yields the $\mu \times t$ phase diagrams at $p = 0.15$ shown in Figs. 8 to 10, corresponding, respectively, to large, intermediate, and small values of υ.

The phase diagram displays a rich spectrum of phases for larger values of υ, as shown in Fig. 8 for $\upsilon = 0.125$. At very low-salt concentrations, the model membrane remains charged (D, standing for dissociated) in both the gel (DG) and the fluid (DF) phases. At intermediate salt concentrations, there is charge ordering on the model membrane for a restricted range of μ: the gel-fluid transition occurs mainly between two semidissociated (SG and SF) charge-ordered phases, but there are also first-order transitions between the SG and the AF or DF phases: Note that this classification is somewhat arbitrary for higher temperatures, and one may simply label them by F. Beyond the first-order main transition, as temperature is increased, a transition temperature is reached at which charge becomes disordered, corresponding to the transition SF-F. Interestingly, the anomalous transition region observed in the relevant experimental system to this model also occurs at intermediate salt concentrations [18], which we propose to be correlated with the existence of charge-ordered phases, in view of the obtained results of the theoretical model. At even higher salt concentrations, $\mu > 0$, the system is fully associated (A) and the usual main gel-fluid (AG-AF) first-order transition of neutral lipids is recovered, similarly as observed in the experimental system [14,18,23–27].

As the Coulomb interaction υ is made less important for fixed lateral pressure p, the SF phase of Fig. 8 moves progressively toward lower temperatures, until the two critical end points collapse and the SF-phase region disappears, but
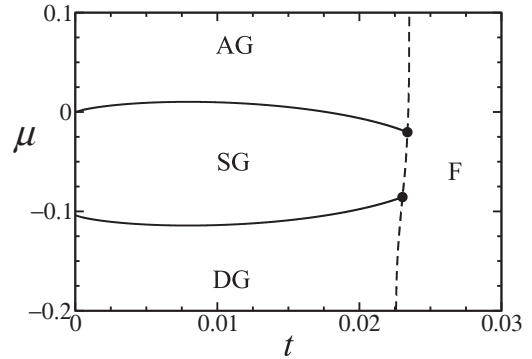

FIG. 9. Typical mean-field phase diagram in the $\mu \times t$ plane for intermediate electrostatic interaction ($\upsilon = 0.08$) and standard values of parameters (λ, ω, p). The meaning of the different lines, black circles, and the two-letter regions are the same as described in the caption to Fig. 8. Compared to Fig. 8, one notices the disappearance of the high-temperature charge-ordered SF phase and the associated second-order transitions. Since it is not possible to distinguish between the AF and DF phases, the high-temperature region is denoted simply by F (fluid).

the SG gel phase remains ordered from the point of view of counterion adsorption (see Fig. 7) for a finite range of values of υ. Therefore, as shown in Fig. 9 for a typical intermediate value $\upsilon = 0.08$, the stable charge-ordered S phase disappears in the fluid (high-temperature) region. For this intermediate value of υ, only the low-temperature gel phase presents the three possibilities, as seen in Fig. 9: a dissociated packed DG membrane at low-salt concentrations, a semidissociated SG (charge-ordered) surface at intermediate ionic strengths, and a predominantly associated AG neutral surface at high-salt concentrations.

As υ is lowered further, the charge-ordered gel phase is driven beyond the gel-fluid transition, as shown in Fig. 10 for a typical small value $\upsilon = 0.05$. Thus, at a low-enough value of the electrostatic repulsion parameter υ, a SG charge-ordered gel phase appears only at very low temperatures, and the main
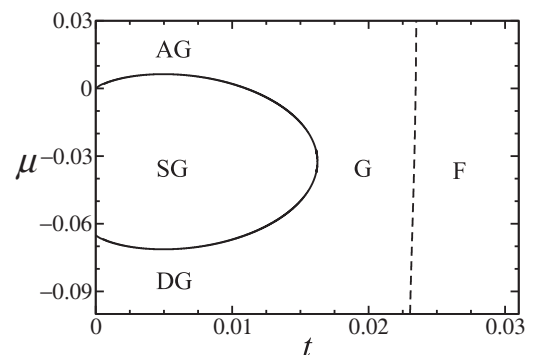

FIG. 10. Typical mean-field phase diagram in the $\mu \times t$ plane for weak electrostatic interaction ($\upsilon = 0.05$) and standard values of parameters (λ, ω, p). The meaning of the different lines and the two-letter regions are the same as described in the caption to Fig. 8. Compared to Fig. 9, one notices the retraction of the charge-ordered SG phase to lower temperatures with the simultaneous disappearance of the critical end points. As in Fig. 9, the high-temperature region is denoted simply by F (fluid).

gel-fluid transition is unaffected by the presence of counterion dissociation.

From the point of view of the global phase diagram, the main gel-fluid transition at the melting temperature T_m, for larger values of μ, is very slightly affected by the salt concentration. For lower values of μ, there is a small shift of T_m toward larger values with increasing ionic strength, which is to be expected [89]. However, the role of the Coulomb interaction is crucial in order to produce the charge-ordered surface in the fluid phase. The dimensionless parameter υ measures the competition between the repulsive electrostatic interaction $\tilde{V}/d_F$ and the effective attractive van der Waals interaction J/γ between acyl chains. If the Coulomb effect is large, both the gel and the fluid regions may present charge-ordered phases. For low-enough υ, the fluid phase is always charge disordered. For even lower υ, both the gel and the fluid phases may remain charge disordered, except at very low temperatures. This can be rationalized as follows: If the effective van der Waals hydrophobic attraction, which drives the order-disorder lipid-chain main transition, is larger (e.g., for longer-chain lipids), the competition parameter υ remains small, and no charge order is seen. Within our interpretation of the model features, this is indeed observed experimentally for dispersions of the ionic lipid DPPG [14,20–22], for which the anomalous transition region almost disappears, contrary to the case of suspensions of the shorter DMPG, which show a wide anomalous region. As hydrophobic attraction is made smaller, the electrostatic repulsion, which would drive headgroups apart, becomes important and may yield charge order in the gel or even in both the gel and the fluid phases. In summary, decreasing the electrostatic interaction υ moves the charge-ordered phases toward lower temperatures until they eventually disappear, as well as shrinks the width of their region of occurrence in the ground-state phase diagram, as depicted in Fig. 4.

Inspection of the effective model Hamiltonian, Eq. (5), shows that the coupling between the two Ising models is controlled by coefficients λ_1 and λ_2, dependent on λ. If λ decreases, approaching 1, which means smaller area differences between the fluid and gel phases, these couplings vanish and the two types of order, acyl-chain and headgroup charge order, fully decouple. On the other hand, a look at the ground-state phase diagram, Fig. 4, shows that the width of the SG phase increases for larger values of $\lambda\upsilon$. Combined with the information displayed in Figs. 8 to 10, this leads to the conclusion that raising λ increases the coupling between the charge and chain degrees of freedom. This is similar to the effect of increasing the electrostatic to hydrophobic interaction, υ. Both induce the possibility of discontinuity of the critical charge-ordering lines, which is a characteristic feature of the coupling. Thus, the role of increasing λ or υ is similar, and decoupling occurs at limiting values of either variable.

C. Model thermodynamics: specific heat and degree of ionization

It is well known that the main gel-fluid transition associated with the disordering of zwitterionic lipid chains may be detected from a DSC peak. This peak develops into a shoulder across an anomalous transition region, in the case of ionic lipids with shorter chains at low ionic strength [11,18]. So what happens in the case of our model of ionic-lipid particles?
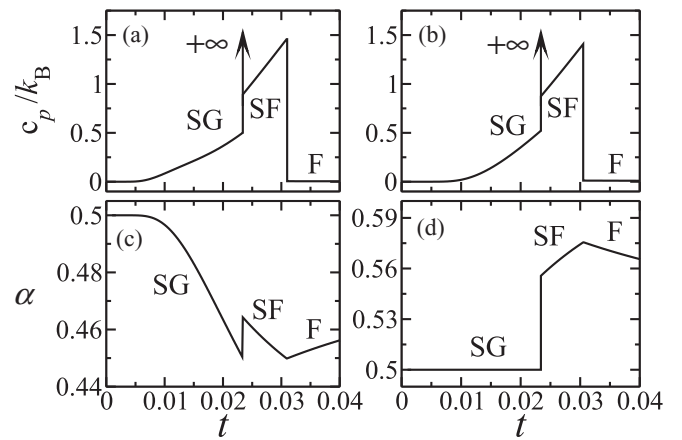

FIG. 11. Strong electrostatic interaction ($\upsilon = 0.125$) specific heat at constant lateral pressure [(a) and (b)] in unities of k_B and degree of ionization α [(c) and (d)] for standard values of parameters (λ, ω, p) as a function of the dimensionless temperature t for $\mu = -0.05$ [left column, (a) and (c)] and $\mu = -0.08125$ [right column, (b) and (d)]. Note the discontinuous (first-order) SG-SF transition and the continuous (second-order) SF-F transition at higher temperatures. The order parameter α has a nonmonotonic behavior as a function of the temperature. After the main SG-SF transition, α reaches a minimum for $\mu = -0.05$ and develops a maximum for $\mu = -0.08125$, both at the second-order transition.

It is interesting to look at the specific-heat profile of the model system (at constant lateral pressure [90] Π and chemical potential of counterions μ_c),

$$\frac{1}{k_B}c_p \equiv \frac{T}{2Nk_B}\left(\frac{\partial S}{\partial T}\right)_{\Pi,2N,\mu_c} = -\frac{t}{J}\left(\frac{\partial^2 \psi}{\partial t^2}\right)_{p,\mu}, \quad (27)$$

in the region of intermediate salt concentration, at which charge-ordered phases arise. Figure 11, for large υ, shows that the gel-fluid transition is accompanied by a divergence of the specific heat, whereas the charge-ordered fluid SF phase contributes with a shoulder that disappears at a charge-disordering second-order transition at higher temperatures. The width of the shoulder depends on added salt (through μ) and decreases as counterion density increases, entirely analogous with the experimental system DMPG (see the Introduction).

Ionic-lipid dispersions may also present a *maximum* in the experimental conductivity curve in the anomalous transition region, in the case of shorter chains, as, e.g., in DMPG [10,17]. Conductivity depends both on the degree of ionization of the macroions as well as on their mobility. A recent study that adds electrophoretic mobility data to the study of conductivity [17] yields a profile for the degree of the lipid vesicle ionization that presents a steep rise at the main transition, followed by increasing dissociation across the anomalous region, at the end of which its degree of ionization diminishes substantially. The degree of ionization predicted for the present model, measured by the order parameter α, is also shown in Fig. 11. It rises discontinuously at the gel-fluid transition, as expected from the discussion of the phase diagram of Fig. 8. Above this first-order transition, the degree of ionization α varies continuously and undergoes an extremum at the continuous charge-disordering transition. Whether the α profile falls or
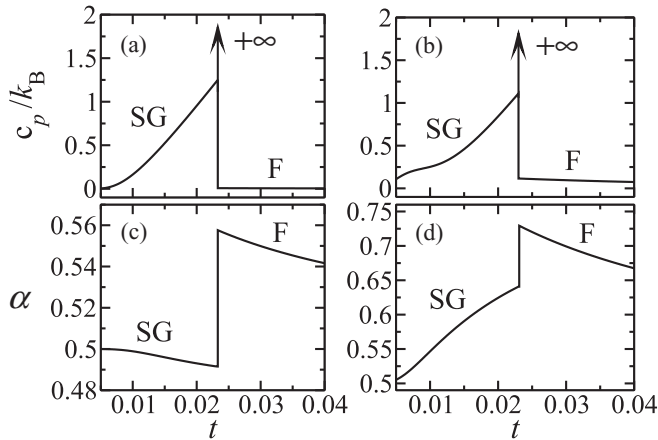
FIG. 12. Intermediate electrostatic interaction ($\upsilon = 0.08$) specific heat at constant lateral pressure [(a) and (b)] in unities of k_{B} and degree of ionization α [(c) and (d)] for standard values of parameters (λ, ω, p) as a function of the dimensionless temperature t for $\mu = -0.05$ [left column, (a) and (c)] and $\mu = -0.08125$ [right column, (b) and (d)]. Note the discontinuous (first-order) SG-F transition. The order parameter α has a nonmonotonic behavior as a function of the temperature. As the SF phase disappeared, there is no additional continuous (second-order) transition at higher temperatures, although the discontinuous rise of α at the main transition remains.

rises after this second transition depends on the value of μ. Larger values of μ lead to α profiles with a minimum, while a maximum is found for lower values of μ. However, in both cases a local maximum is present in the temperature region for which specific heat presents a shoulder, interpreted as the anomalous transition region.

If the effect of the Coulomb interaction υ is made smaller, the shoulder in the specific heat disappears, while degree of ionization α presents a discontinuity at the main transition, as shown in Figs. 12 and 13 for $\upsilon = 0.08$ and $\upsilon = 0.05$, respectively. Thus an "anomalous transition region" is absent if the headgroup Coulomb interaction is made less important with respect to hydrophobic chain attraction. As pointed out in the previous subsection and in the Introduction, this would be the case for longer lipid chains, such as DSPG.

VI. CONCLUDING REMARKS

The model presented in this work combines attractive nonelectrostatic and repulsive Coulomb interactions between bilayer-forming charged lipids in the presence of a counterion reservoir. The nonelectrostatic part is accounted for by using effective van der Waals parameters associated with net attractive interactions between distinct states of the lipid acyl chains. Even though our model relies on several parameters that cannot be directly accessed solely by experimental techniques, it presents a rich thermodynamic behavior, which might be compared to experimental measurements on vesicle or lamellae-forming ionic lipid suspensions. In fact, we show that by fitting some of the effective theoretical parameters in order to reproduce some experimental data on real systems under restricted constraints, the theoretical results resemble the experimental measurements of the thermotropic behavior
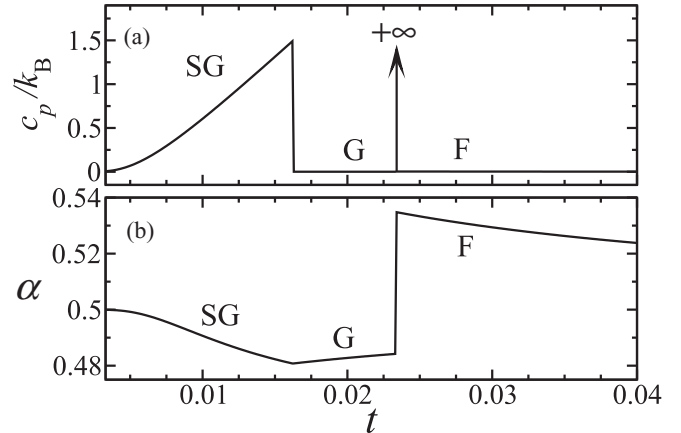

FIG. 13. Weak electrostatic interaction ($\upsilon = 0.05$) specific heat at constant lateral pressure (a) in unities of k_{B} and degree of ionization α (b) for standard values of parameters (λ, ω, p) as a function of the dimensionless temperature t for $\mu = -0.03$. Note the continuous (second-order) SG-G transition at lower temperatures and the discontinuous (first-order) G-F transition at higher temperatures. The order parameter α has a nonmonotonic behavior as a function of the temperature.

of the specific heat and degree of ionization, as done in a companion work [88].

We believe that the emergent properties obtained in this work may be relevant to some experimental systems. Indeed, the model is motivated by the experimentally observed anomalous transition region in suspensions of ionic lipids with short acyl chains in low ionic strengths [18]. We suggest that the typical results offer a qualitative explanation for this peculiar behavior. The presence of charge-ordered phases, associated with the release of a large fraction of the counterions to the aqueous solution, represents a mechanism that might explain the experimentally observed conductivity profile in this transition region. Therefore, the main result of our calculations—the existence of semidissociated phases for intermediate salt concentrations—supports a broad transition region that evolves to a single first-order sharp transition in high-ionic strengths, analogous to the neutral-lipid case. Our model predicts that for a sufficient amount of salt, as well as for long-enough acyl chains, the charge-ordered phase and the associated anomalous transition region disappear altogether. The main effect of the added salt is to modulate (shrink and even eliminate) the charge-ordered phases.

Besides their extended and ordered acyl chains, PG lipids in the gel phase arrange, usually, in a regular orthorhombic lattice [27,49,91]. However, depending on the preparation conditions, the chains in the gel phase may also adopt a hexagonal packing [91]. For the standard Ising antiferromagnet in a magnetic field, the ordered state on a triangular lattice is highly nontrivial due to frustration and cannot be simply described as a two-sublattice staggered state [92]. Most likely, this feature has consequences on our model when considered on a triangular lattice, associated with a hexagonal-packing gel phase. The study of this question is beyond the scope of the present work and it might be a topic for future work.

Due to the simplified nature of the theoretical model, our predictions should be regarded as a tentative explanation of the

underlying mechanism behind the experimentally observed complex behavior. In particular, we treated the system as lamellar, while there are indications of drastic conformational changes in the anomalous transition region, in analogy to the rich polymorphism observed in single-component as well as in mixed-lipid aqueous dispersions [93]. In fact, several competing models, based on many complementary experimental techniques, have been proposed for DMPG aqueous suspensions: perforated bicelles (bilayered micelles) [5], deformed [9] and/or perforated vesicles [11,12], spongelike connected networks [13,14,21], and bilayer fragments and/or bicelles [15], none of which approach the effect of counterion association. Thus, we hope that our discussion may shed some light on the microscopic origin of the rich thermodynamic behavior of aqueous suspensions of ionic lipids. A less qualitative comparison with experiments requires the coupling of the acyl-chain order-disorder phase transitions in the bilayer plane with the electrostatic interactions in the bulk aqueous suspension. The latter can be treated using the Poisson-Boltzmann theory for ionic solutions [94], coupling the charged lamellar system to a reservoir of symmetric monovalent salt, as performed for semiphenomenological models for charged multilamellar systems [95,96], and lamellar phases [97] or monolayers [98] composed of anion-adsorbing zwitterionic lipids. This question deserves further investigation and is currently in progress.

APPENDIX A: MEAN-FIELD EQUATIONS VIA GAUSSIAN TRANSFORMATION

The effective Hamiltonian per lipid in the $(T,\Pi,2N,\mu_c)$ ensemble is written in simplified form as

$$\frac{1}{2N}\mathcal{H}_{\text{eff}} = \varphi_0(t) + \varphi_1 + \varphi_2, \tag{A1}$$

$$\beta\varphi_1 = \frac{1}{2t}\sum_{\nu=1,2}(h_\nu m_\nu + \mu_\nu \alpha_\nu - \theta_\nu q_\nu), \tag{A2}$$

$$\beta\varphi_2 = -\frac{2}{t}m_1 m_2 + \frac{\upsilon}{2t}[\alpha_1\alpha_2 + \lambda_1 q_1 q_2 + \lambda_2(\alpha_1 q_2 + \alpha_2 q_1)], \tag{A3}$$

with the sublattice averages (m_ν,α_ν,q_ν) defined by Eqs. (8) and the model parameters $(h_\nu,\mu_\nu,\theta_\nu)$ by Eqs. (12).

In order to diagonalize the quadratic form represented by φ_2, we define the overall lattice averages, Eqs. (9), as well as the staggered averages, Eqs. (10), which represent the thermodynamic order parameters. These definitions allow rearrangement of Hamiltonian terms, so φ_2 becomes diagonal,

$$\beta\varphi_1 = \frac{1}{2t}[(h_1+h_2)m + (h_1-h_2)m^\dagger + (\mu_1+\mu_2)\alpha + (\mu_1-\mu_2)\alpha^\dagger - (\theta_1+\theta_2)q - (\theta_1-\theta_2)q^\dagger], \tag{A4}$$

$$\beta\varphi_2 = -k_x(m^2 - m^{\dagger 2}) + k_y[(\alpha + \lambda_2 q)^2 - (\alpha^\dagger + \lambda_2 q^\dagger)^2] + k_z(q^2 - q^{\dagger 2}), \tag{A5}$$

with parameters

$$k_x \equiv \frac{2}{t}, \quad k_y \equiv \frac{\upsilon}{2t}, \quad k_z \equiv k_y(\lambda_1 - \lambda_2^2) = \frac{\lambda\upsilon}{2t}\left(\frac{\lambda-1}{\lambda+1}\right)^2. \tag{A6}$$

A sixfold Gaussian transformation

$$e^{\pm k\eta^2} = \sqrt{k/\pi}\int_{-\infty}^{\infty}dx\, e^{-kx^2 + 2\eta kx\sqrt{\pm 1}}, \tag{A7}$$

may be then applied to $e^{-\beta\mathcal{H}_{\text{eff}}}$ in order to linearize the quadratic terms,

$$e^{-\beta\mathcal{H}_{\text{eff}}} = \left(\frac{N}{\pi t}\right)^3 \frac{\lambda\upsilon^2}{2}\left(\frac{\lambda-1}{\lambda+1}\right)^2 \int d^6\boldsymbol{r}\, e^{-2N\beta\Phi}, \tag{A8}$$

$$\beta\Phi = \beta\varphi_0(t) + k_x(x^2 + x^{\dagger 2}) + k_y(y^2 + y^{\dagger 2}) + k_z(z^2 + z^{\dagger 2})$$
$$+ \left[\frac{1}{2t}(h_1+h_2) - 2k_x x\right]m + \left[\frac{1}{2t}(h_1-h_2) + 2k_x\frac{x^\dagger}{i}\right]m^\dagger$$
$$+ \left[\frac{1}{2t}(\mu_1+\mu_2) + 2k_y\frac{y}{i}\right]\alpha + \left[\frac{1}{2t}(\mu_1-\mu_2) - 2k_y y^\dagger\right]\alpha^\dagger$$
$$- \left[\frac{1}{2t}(\theta_1+\theta_2) - 2\lambda_2 k_y\frac{y}{i} - 2k_z\frac{z}{i}\right]q$$
$$- \left[\frac{1}{2t}(\theta_1-\theta_2) + 2\lambda_2 k_y y^\dagger + 2k_z z^\dagger\right]q^\dagger, \tag{A9}$$

with $\boldsymbol{r} \equiv (x,y,z,x^\dagger,y^\dagger,z^\dagger)$. The linearized exponential factor leads to a factorization of the associated partition function $\Xi_{2N}(T,\Pi,\mu_c)$, Eq. (3). This allows the trace to be exactly performed, since the summation over all possible particle-state lattice configurations decouples into independent summations over single-site states,

$$\sum_{\{s_i\},\{\tau_i\}} e^{-2N\beta\Phi} = (\xi_1\xi_2)^N \exp\Big\{-2N\big[\beta\varphi_0(t)$$
$$+ k_x(x^2 + x^{\dagger 2}) + k_y(y^2 + y^{\dagger 2})$$
$$+ k_z(z^2 + z^{\dagger 2})\big]\Big\},$$
$$\xi_\nu \equiv \sum_{s,\tau\in\nu} e^{\beta\phi_{s\tau}^{(\nu)}}, \tag{A10}$$

$$\beta\phi_{s\tau}^{(\nu)} \equiv -s\left\{\frac{h_\nu}{t} - 2k_x\left[x + (-1)^\nu\frac{x^\dagger}{i}\right]\right\}$$
$$- \tau\left\{\frac{\mu_\nu}{t} + 2k_y\left[\frac{y}{i} + (-1)^\nu y^\dagger\right]\right\}$$
$$+ s\tau\left\{\frac{\theta_\nu}{t} - 2\lambda_2 k_y\left[\frac{y}{i} + (-1)^\nu y^\dagger\right]\right.$$
$$\left. - 2k_z\left[\frac{z}{i} + (-1)^\nu z^\dagger\right]\right\}. \tag{A11}$$

Therefore, the associated partition function reads

$$\Xi_{2N}(T,\Pi,\mu_c) = \sum_{\{s_i\},\{\tau_i\}} e^{-\beta\mathcal{H}_{\text{eff}}} = \left(\frac{N}{\pi t}\right)^3 \frac{\lambda\upsilon^2}{2}\left(\frac{\lambda-1}{\lambda+1}\right)^2$$
$$\times \int d^6\boldsymbol{r}\, e^{-\beta\Psi_{2N}(T,\Pi,\mu_c;\boldsymbol{r})}, \tag{A12}$$

with the mean-field free-energy functional per lipid in the thermodynamic limit $\Psi \equiv \lim_{N\to\infty} \frac{1}{2N} \Psi_{2N}(T,\Pi,\mu_c; \boldsymbol{r})$ given by

$$\beta\Psi(T,\Pi,\mu_c; \boldsymbol{r}) = \beta\varphi_0(t) + k_x(x^2 + x^{\dagger 2}) + k_y(y^2 + y^{\dagger 2}) + k_z(z^2 + z^{\dagger 2})$$

$$- \frac{1}{2}\ln\left\{1 + \exp\left[-\frac{h_1}{t} + 2k_x\left(x - \frac{x^\dagger}{i}\right)\right] + \exp\left[-\frac{\mu_1}{t} - 2k_y\left(\frac{y}{i} - y^\dagger\right)\right]\right.$$

$$\left. + \exp\left[-\frac{h_1}{t} - \frac{\mu_1}{t} + \frac{\theta_1}{t} + 2k_x\left(x - \frac{x^\dagger}{i}\right) - 2k_y(1+\lambda_2)\left(\frac{y}{i} - y^\dagger\right) - 2k_z\left(\frac{z}{i} - z^\dagger\right)\right]\right\}$$

$$- \frac{1}{2}\ln\left\{1 + \exp\left[-\frac{h_2}{t} + 2k_x\left(x + \frac{x^\dagger}{i}\right)\right] + \exp\left[-\frac{\mu_2}{t} - 2k_y\left(\frac{y}{i} + y^\dagger\right)\right]\right.$$

$$\left. + \exp\left[-\frac{h_2}{t} - \frac{\mu_2}{t} + \frac{\theta_2}{t} + 2k_x\left(x + \frac{x^\dagger}{i}\right) - 2k_y(1+\lambda_2)\left(\frac{y}{i} + y^\dagger\right) - 2k_z\left(\frac{z}{i} + z^\dagger\right)\right]\right\}. \quad \text{(A13)}$$

The integrations in Eq. (A12) are performed using the steepest-descent method. The stationary-point conditions of the functional $\nabla\Psi(\boldsymbol{r} = \bar{\boldsymbol{r}}) = \boldsymbol{0}$ for the six-dimensional stationary points $\bar{\boldsymbol{r}} \equiv (\bar{x}, \bar{y}, \bar{z}, \bar{x}^\dagger, \bar{y}^\dagger, \bar{z}^\dagger)$ connect them with the physical sublattice averages,

$$m_\nu = \langle s \rangle_\nu = -\frac{2}{\Delta a} \frac{\partial \psi}{\partial \Pi_\nu}, \quad \alpha_\nu = \langle \tau \rangle_\nu = 1 + 2\frac{\partial \psi}{\partial \mu_\nu^c},$$
(A14)
$$q_\nu = \langle s\tau \rangle_\nu = -2\frac{\partial \psi}{\partial \Theta_\nu},$$

$$\bar{x} \pm \frac{\bar{x}^\dagger}{i} = m_{1,2}, \quad \frac{\bar{y}}{i} \pm \bar{y}^\dagger = \alpha_{1,2} + \lambda_2 q_{1,2}, \quad \frac{\bar{z}}{i} \pm \bar{z}^\dagger = q_{1,2}.$$
(A15)

The equations of state (20) and the fields $\phi_{s\tau}^{(\nu)}$, Eqs. (22)–(24), correspond, respectively, to Eqs. (A14) and (A15) and Eq. (A11) expressed in terms of the lattice thermodynamic averages $(m_\nu, \alpha_\nu, q_\nu)$. Replacing them into the mean-field free-energy functional, Eq. (A13), one obtains the thermodynamic free energy per lipid $\psi(T,\Pi,\mu_c) = \Psi(T,\Pi,\mu_c; \boldsymbol{r} = \bar{\boldsymbol{r}})$ given by Eq. (25).

APPENDIX B: MEAN-FIELD EQUATIONS VIA DIRAC-δ-FUNCTION REPRESENTATION

The effective Hamiltonian per lipid in the $(T,\Pi,2N,\mu_c)$ ensemble is written in simplified form as

$$\frac{1}{2N}\mathcal{H}_{\text{eff}} = \varphi_0(t) + \varphi_1 + \varphi_2, \quad \text{(B1)}$$

$$\beta\varphi_1 = \frac{1}{2N} \sum_{\nu=1,2} \sum_{\substack{i=1 \\ i\in\nu}}^{N} \frac{1}{t}(h_\nu s_i + \mu_\nu \tau_i - \theta_\nu s_i \tau_i), \quad \text{(B2)}$$

$$\beta\varphi_2 = -k_x m_1 m_2 + k_y[\alpha_1\alpha_2 + \lambda_1 q_1 q_2 + \lambda_2(\alpha_1 q_2 + \alpha_2 q_1)]. \quad \text{(B3)}$$

By introducing the continuous complex fields $\boldsymbol{R}_\nu \equiv (X_\nu, Y_\nu, Z_\nu)$ conjugated to the sublattice averages $(m_\nu, \alpha_\nu, q_\nu)$, which are defined by the Dirac-δ-function representations

$$\delta\left(m_\nu - \frac{1}{N}\sum_{\substack{i=1 \\ i\in\nu}}^{N} s_i\right) = \frac{N}{2\pi i} \int_{-i\infty}^{i\infty} dX_\nu$$
$$\times \exp\left[-NX_\nu\left(m_\nu - \frac{1}{N}\sum_{\substack{i=1 \\ i\in\nu}}^{N} s_i\right)\right], \quad \text{(B4)}$$

$$\delta\left(\alpha_\nu - \frac{1}{N}\sum_{\substack{i=1 \\ i\in\nu}}^{N} \tau_i\right) = \frac{N}{2\pi i} \int_{-i\infty}^{i\infty} dY_\nu$$
$$\times \exp\left[-NY_\nu\left(\alpha_\nu - \frac{1}{N}\sum_{\substack{i=1 \\ i\in\nu}}^{N} \tau_i\right)\right], \quad \text{(B5)}$$

$$\delta\left(q_\nu - \frac{1}{N}\sum_{\substack{i=1 \\ i\in\nu}}^{N} s_i\tau_i\right) = \frac{N}{2\pi i} \int_{-i\infty}^{i\infty} dZ_\nu$$
$$\times \exp\left[-NZ_\nu\left(q_\nu - \frac{1}{N}\sum_{\substack{i=1 \\ i\in\nu}}^{N} s_i\tau_i\right)\right], \quad \text{(B6)}$$

it is possible to rewrite $e^{-\beta\mathcal{H}_{\text{eff}}}$ as

$$e^{-\beta\mathcal{H}_{\text{eff}}}$$
$$= \left(\frac{N}{2\pi i}\right)^6 \left[\prod_{\nu=1,2} \int_{-i\infty}^{i\infty} d^3\boldsymbol{R}_\nu \int_{-\infty}^{\infty} dm_\nu \, d\alpha_\nu \, dq_\nu\right] e^{-2N\beta\Phi}, \quad \text{(B7)}$$

$$\Phi = \varphi_0(t) + \varphi_2 + \frac{1}{2\beta} \sum_{\nu=1,2} (X_\nu m_\nu + Y_\nu \alpha_\nu + Z_\nu q_\nu)$$

$$- \frac{1}{2N} \sum_{\nu=1,2} \sum_{\substack{i=1 \\ i \in \nu}}^{N} \phi_{s_i \tau_i}^{(\nu)}, \qquad (B8)$$

$$\beta \phi_{s\tau}^{(\nu)} \equiv -s\left(\frac{h_\nu}{t} - X_\nu\right) - \tau\left(\frac{\mu_\nu}{t} - Y_\nu\right) + s\tau\left(\frac{\theta_\nu}{t} + Z_\nu\right). \qquad (B9)$$

Since Φ is linear in the particle-state variables $\{s_i, \tau_i\}$, the trace can be exactly performed, since the summation over all possible particle-state lattice configurations decouples into independent summations over single-site states,

$$\sum_{\{s_i\},\{\tau_i\}} e^{-2N\beta\Phi} = e^{-2N[\beta\varphi_0(t)+\beta\varphi_2]} \prod_{\nu=1,2} \xi_\nu^N e^{-N(X_\nu m_\nu + Y_\nu \alpha_\nu + Z_\nu q_\nu)},$$
$$\qquad (B10)$$
$$\xi_\nu \equiv \sum_{s,\tau \in \nu} e^{\beta\phi_{s\tau}^{(\nu)}},$$

which allows the associated partition function to be written as

$$\Xi_{2N} = \sum_{\{s_i\},\{\tau_i\}} e^{-\beta\mathcal{H}_{\text{eff}}}$$

$$= \left(\frac{N}{2\pi i}\right)^6 \left[\prod_{\nu=1,2} \int_{-i\infty}^{i\infty} d^3\mathbf{R}_\nu \int_{-\infty}^{\infty} dm_\nu \, d\alpha_\nu \, dq_\nu\right] e^{-\beta\Psi_{2N}(\mathbf{R}_\nu)},$$
$$\qquad (B11)$$

with the mean-field free-energy functional per lipid in the thermodynamic limit $\Psi(\mathbf{R}_\nu) \equiv \lim_{N\to\infty} \frac{1}{2N} \Psi_{2N}(\mathbf{R}_\nu)$ given by

$$\beta\Psi(\mathbf{R}_\nu) = \beta\varphi_0(t) + \beta\varphi_2 + \frac{1}{2} \sum_{\nu=1,2} (X_\nu m_\nu + Y_\nu \alpha_\nu + Z_\nu q_\nu)$$

$$- \frac{1}{2}\ln\left[1 + \exp\left(-\frac{h_1}{t} + X_1\right) + \exp\left(-\frac{\mu_1}{t} + Y_1\right)\right.$$

$$\left. + \exp\left(-\frac{h_1}{t} - \frac{\mu_1}{t} + \frac{\theta_1}{t} + X_1 + Y_1 + Z_1\right)\right]$$

$$- \frac{1}{2}\ln\left[1 + \exp\left(-\frac{h_2}{t} + X_2\right) + \exp\left(-\frac{\mu_2}{t} + Y_2\right)\right.$$

$$\left. + \exp\left(-\frac{h_2}{t} - \frac{\mu_2}{t} + \frac{\theta_2}{t} + X_2 + Y_2 + Z_2\right)\right]. \quad (B12)$$

In the thermodynamic limit $N \to \infty$, the integrations over the continuous complex fields $\mathbf{R}_\nu$ may be performed by the steepest-descent method. The saddle-point conditions $\nabla_\nu \Psi = \mathbf{0}$, with $\nabla_\nu \equiv \left(\frac{\partial}{\partial X_\nu}, \frac{\partial}{\partial Y_\nu}, \frac{\partial}{\partial Z_\nu}\right)$, yield the self-consistent sublattice averages, $(m_\nu, \alpha_\nu, q_\nu) = \nabla_\nu \ln \xi_\nu$,

$$m_\nu = \frac{1}{\xi_\nu} \sum_{s,\tau \in \nu} s \, e^{\beta\phi_{s\tau}^{(\nu)}} \equiv \langle s \rangle_\nu, \quad \alpha_\nu = \frac{1}{\xi_\nu} \sum_{s,\tau \in \nu} \tau \, e^{\beta\phi_{s\tau}^{(\nu)}} \equiv \langle \tau \rangle_\nu,$$
$$\qquad (B13)$$
$$q_\nu = \frac{1}{\xi_\nu} \sum_{s,\tau \in \nu} s\tau \, e^{\beta\phi_{s\tau}^{(\nu)}} \equiv \langle s\tau \rangle_\nu.$$

In principle, this set of equations allows one to express the saddle points $\bar{\mathbf{R}}_\nu \equiv (\bar{X}_\nu, \bar{Y}_\nu, \bar{Z}_\nu)$ in terms of the lattice averages $(m_\nu, \alpha_\nu, q_\nu)$.

Performing the integrations over the continuous variables $(m_\nu, \alpha_\nu, q_\nu)$ by the steepest-descent method, one may show that the stationary-point conditions of the functional $\partial\Psi/\partial m_\nu = \partial\Psi/\partial\alpha_\nu = \partial\Psi/\partial q_\nu = 0$ reduce, for the sublattice $\nu = 1$, to the linear relations

$$\bar{X}_1 = -2\beta\frac{\partial\varphi_2}{\partial m_1} = 2k_x m_2 = \frac{4}{t}m_2, \qquad (B14)$$

$$\bar{Y}_1 = -2\beta\frac{\partial\varphi_2}{\partial\alpha_1} = -2k_y(\alpha_2 + \lambda_2 q_2) = -\frac{\upsilon}{t}\left(\alpha_2 + \frac{\lambda-1}{\lambda+1}q_2\right), \qquad (B15)$$

$$\bar{Z}_1 = -2\beta\frac{\partial\varphi_2}{\partial q_1} = -2k_y(\lambda_2\alpha_2 + \lambda_1 q_2)$$

$$= -\frac{\upsilon}{t}\left(\frac{\lambda-1}{\lambda+1}\right)[\alpha_2 + (\lambda-1)q_2], \qquad (B16)$$

since contributions from the logarithmic terms cancel out due to the saddle-point conditions, Eqs. (B13). Equations for the stationary-point conditions for the sublattice $\nu = 2$ yield relations of the same form but switching the sublattice labels $1 \to 2$ and $2 \to 1$ in the final expressions of Eqs. (B14)–(B16). Replacing the saddle points, Eqs. (B14)–(B16) and their analogs for the sublattice $\nu = 2$, into the mean-field free-energy functional, Eq. (B12), order parameters, Eqs. (B13), and fields $\phi_{s\tau}^{(\nu)}$, Eq. (B9), one regains Eq. (25) and Eqs. (20)–(24). Of course, this method yields exactly the same results of Appendix A.

APPENDIX C: MEAN-FIELD ANALYSIS OF THE GROUND STATE

The ground-state energies are given in terms of the energy parameters $\varphi_0(t = 0) \equiv -\mu_c + \epsilon_F - \gamma\epsilon_{FF}/2 + \Pi a_F$, $J \equiv \gamma(\epsilon_{GG} + \epsilon_{FF} - 2\epsilon_{GF})/4$ and the dimensionless couplings $p \equiv (2\Pi\Delta a + \Delta\epsilon)/4J$, $\mu \equiv \mu_c/J$, $\theta \equiv \Theta/J$.

1. AF mean-field ground state ($m = 0, \alpha = 0, q = 0$), leading term: $\phi_{00} = 0$

Zero-temperature asymptotic limit

$$\phi_{10} = 2J(p-1), \quad \phi_{01} = -J\mu, \quad \phi_{11} = J(2p-2-\mu), \qquad (C1)$$

$$\Delta\psi_0(0,0,0) \equiv \psi_0(0,0,0) - \varphi_0(t=0) = 0. \qquad (C2)$$

Conditions for existence of the AF ground state

$$\phi_{10} < 0 : p < 1, \quad \phi_{01} < 0 : \mu > 0,$$
$$\phi_{11} < 0 : \mu > 2(p-1). \qquad (C3)$$

2. AG mean-field ground state ($m = 1, \alpha = 0, q = 0$), leading term: ϕ_{10}

Zero-temperature asymptotic limit

$$\phi_{10} = 2J(p+1), \quad \phi_{01} = -J\mu, \quad \phi_{11} = J(2p+2-\mu), \qquad (C4)$$

$$\Delta\psi_0(1,0,0) \equiv \psi_0(1,0,0) - \varphi_0(t=0) = -2Jp. \quad \text{(C5)}$$

Conditions for existence of the AG ground state

$$\phi_{10} > 0 : p > -1, \quad \phi_{10} > \phi_{01} : \mu > -2(p+1),$$
$$\phi_{10} > \phi_{11} : \mu > 0. \quad \text{(C6)}$$

3. DF mean-field ground state ($m = 0, \alpha = 1, q = 0$), leading term: ϕ_{01}

Zero-temperature asymptotic limit

$$\phi_{10} = 2J(p-1), \quad \phi_{01} = -J(\mu+\upsilon),$$
$$\phi_{11} = J\left(2p - 2 - \mu + \theta - \frac{2\lambda\upsilon}{\lambda+1}\right), \quad \text{(C7)}$$

$$\Delta\psi_0(0,1,0) \equiv \psi_0(0,1,0) - \varphi_0(t=0) = J\left(\mu + \frac{\upsilon}{2}\right). \quad \text{(C8)}$$

Conditions for existence of the DF ground state

$$\phi_{01} > 0 : \mu < -\upsilon, \quad \phi_{01} > \phi_{10} : \mu < -2(p-1) - \upsilon,$$
$$\phi_{01} > \phi_{11} : p < 1 - \frac{\theta}{2} + \frac{\upsilon}{2}\left(\frac{\lambda-1}{\lambda+1}\right). \quad \text{(C9)}$$

4. DG mean-field ground state ($m = 1, \alpha = 1, q = 1$), leading term: ϕ_{11}

Zero-temperature asymptotic limit

$$\phi_{10} = 2J(p+1), \quad \phi_{01} = -J\left(\mu + \frac{2\lambda\upsilon}{\lambda+1}\right),$$
$$\phi_{11} = J(2p + 2 - \mu + \theta - \lambda\upsilon), \quad \text{(C10)}$$

$$\Delta\psi_0(1,1,1) \equiv \psi_0(1,1,1) - \varphi_0(t=0) = -J\left(2p - \mu - \frac{\lambda\upsilon}{2}\right). \quad \text{(C11)}$$

Conditions for existence of the DG ground state

$$\phi_{11} > 0 : \mu < 2(p+1) + \theta - \lambda\upsilon,$$
$$\phi_{11} > \phi_{10} : \mu < \theta - \lambda\upsilon, \quad \text{(C12)}$$
$$\phi_{11} > \phi_{01} : p > -1 - \frac{\theta}{2} + \frac{\lambda\upsilon}{2}\left(\frac{\lambda-1}{\lambda+1}\right).$$

5. SF mean-field ground state ($m_1 = m_2 = 0, \alpha_1 = 1, \alpha_2 = 0, q_1 = q_2 = 0$), leading terms: $\phi_{01}^{(1)}$ and $\phi_{00}^{(2)} = 0$

Zero-temperature asymptotic limit

$$\phi_{10}^{(1)} = 2J(p_1 - 1), \quad \phi_{01}^{(1)} = -J\mu_1,$$
$$\phi_{11}^{(1)} = J(2p_1 - 2 - \mu_1 + \theta_1), \quad \text{(C13)}$$

$$\phi_{10}^{(2)} = 2J(p_2 - 1), \quad \phi_{01}^{(2)} = -J(\mu_2 + \upsilon),$$
$$\phi_{11}^{(2)} = J\left(2p_2 - 2 - \mu_2 + \theta_2 - \frac{2\lambda\upsilon}{\lambda+1}\right), \quad \text{(C14)}$$

$$\Delta\psi_0(0,0;1,0;0,0) \equiv \psi_0(0,0;1,0;0,0) - \varphi_0(t=0) = \frac{J\mu_1}{2}. \quad \text{(C15)}$$

Conditions for existence of the SF ground state

$$\phi_{01}^{(1)} > 0 : \mu_1 < 0, \quad \phi_{01}^{(1)} > \phi_{10}^{(1)} : \mu_1 < -2(p_1 - 1),$$
$$\phi_{01}^{(1)} > \phi_{11}^{(1)} : p_1 < 1 - \frac{\theta_1}{2}, \quad \text{(C16)}$$

$$\phi_{10}^{(2)} < 0 : p_2 < 1, \quad \phi_{01}^{(2)} < 0 : \mu_2 > -\upsilon,$$
$$\phi_{11}^{(2)} < 0 : \mu_2 > 2(p_2 - 1) + \theta_2 - \frac{2\lambda\upsilon}{\lambda+1}. \quad \text{(C17)}$$

6. SG mean-field ground state ($m_1 = m_2 = 1, \alpha_1 = 1, \alpha_2 = 0, q_1 = 1, q_2 = 0$), leading terms: $\phi_{11}^{(1)}$ and $\phi_{10}^{(2)}$

Zero-temperature asymptotic limit

$$\phi_{10}^{(1)} = 2J(p_1 + 1), \quad \phi_{01}^{(1)} = -J\mu_1,$$
$$\phi_{11}^{(1)} = J(2p_1 + 2 - \mu_1 + \theta_1), \quad \text{(C18)}$$

$$\phi_{10}^{(2)} = 2J(p_2 + 1), \quad \phi_{01}^{(2)} = -J\left(\mu_2 + \frac{2\lambda\upsilon}{\lambda+1}\right),$$
$$\phi_{11}^{(2)} = J(2p_2 + 2 - \mu_2 + \theta_2 - \lambda\upsilon), \quad \text{(C19)}$$

$$\Delta\psi_0(1,1;1,0;1,0) \equiv \psi_0(1,1;1,0;1,0) - \varphi_0(t=0)$$
$$= -J\left(2p_1 - \frac{\mu_1}{2} + \frac{\theta_1}{2}\right). \quad \text{(C20)}$$

Conditions for existence of the SG ground state

$$\phi_{11}^{(1)} > 0 : \mu_1 < \theta_1 + 2(p_1 + 1), \quad \phi_{11}^{(1)} > \phi_{10}^{(1)} : \mu_1 < \theta_1,$$
$$\phi_{11}^{(1)} > \phi_{01}^{(1)} : p_1 > -1 - \frac{\theta_1}{2}, \quad \text{(C21)}$$

$$\phi_{10}^{(2)} > 0 : p_2 > -1,$$
$$\phi_{10}^{(2)} > \phi_{01}^{(2)} : \mu_2 > -2(p_2 + 1) - \frac{2\lambda\upsilon}{\lambda+1}, \quad \text{(C22)}$$
$$\phi_{10}^{(2)} > \phi_{11}^{(2)} : \mu_2 > \theta_2 - \lambda\upsilon.$$

[1] J. F. Nagle, Ann. Rev. Phys. Chem. **31**, 157 (1980); G. Cevc and D. Marsh, *Phospholipid Bilayers: Physical Principles and Models* (Wiley Interscience, New York, 1987); D. Marsh, Chem. Phys. Lipids **57**, 109 (1991); G. Cevc (ed.), *Phospholipids Handbook* (Marcel Dekker, New York, 1993); R. Koynova and M. Caffrey, Biochim. Biophys. Acta **1376**, 91 (1998); **1513**, 82 (2001); J. F. Nagle and S. Tristam-Nagle, *ibid* **1469**, 159 (2000); S. Tristam-Nagle and J. F. Nagle, Chem. Phys. Lipids **127**, 3 (2004); T. Heimburg, *Thermal Biophysics of Membranes* (Wiley-VCH, Weinheim, 2007).

[2] K. A. Riske, L. Q. Amaral, and M. T. Lamy-Freund, Biochim. Biophys. Acta **1511**, 297 (2001).

[3] K. A. Riske, L. Q. Amaral, H.-G. Döbereiner, and M. T. Lamy, Biophys. J. **86**, 3722 (2004).

[4] R. M. Fernandez, K. A. Riske, L. Q. Amaral, R. Itri, and M. T. Lamy, Biochim. Biophys. Acta **1778**, 907 (2008).

[5] F. Spinozzi, L. Paccamiccio, P. Mariani, and L. Q. Amaral, Langmuir **26**, 6484 (2010).

[6] K. A. Riske, O. R. Nascimento, M. Peric, B. L. Bales, and M. T. Lamy-Freund, Biochim. Biophys. Acta **1418**, 133 (1999).

[7] K. A. Riske, R. M. Fernandez, O. R. Nascimento, B. L. Bales, and M. T. Lamy-Freund, Chem. Phys. Lipids **124**, 69 (2003).

[8] E. L. Duarte, T. R. Oliveira, D. S. Alves, V. Micol, and M. T. Lamy, Langmuir **24**, 4041 (2008).

[9] J.-M. I. Alakoskela and P. K. J. Kinnunen, Langmuir **23**, 4203 (2007).

[10] K. A. Riske, M. J. Politi, W. F. Reed, and M. T. Lamy-Freund, Chem. Phys. Lipids **89**, 31 (1997).

[11] K. A. Riske, L. Q. Amaral, and M. T. Lamy, Langmuir **25**, 10083 (2009).

[12] J.-M. Alakoskela, M. J. Parry, and P. K. J. Kinnunen, Langmuir **26**, 4892 (2010).

[13] T. Heimburg and R. L. Biltonen, Biochemistry **33**, 9477 (1994).

[14] M. F. Schneider, D. Marsh, W. Jahn, B. Kloesgen, and T. Heimburg, Proc. Natl. Acad. Sci. USA **96**, 14312 (1999).

[15] H. W. Meyer, W. Richter, W. Rettig, and M. Stumpf, Colloids Surf. A **183-185**, 495 (2001).

[16] I. S. Salonen, K. K. Eklund, J. A. Virtanen, and P. K. J. Kinnunen, Biochim. Biophys. Acta **982**, 205 (1989).

[17] R. P. Barroso, K. A. Riske, V. B. Henriques, and M. T. Lamy, Langmuir **26**, 13805 (2010).

[18] M. T. Lamy-Freund and K. A. Riske, Chem. Phys. Lipids **122**, 19 (2003).

[19] Henceforth we will use the conventional four-letter abbreviations for phospholipids with doubly saturated acyl chains of the form DXPY, where the second letter X labels the length of the two identical saturated acyl (or diacyl) chains of each lipid and the fourth letter Y specifies the type of polar headgroup. The lengths of the acyl chains cited in this work, measured by the number of carbon atoms, are given by L = 12 (lauroyl), M = 14 (myristoyl), P = 16 (palmitoyl), and S = 18 (stearoyl). Examples of polar headgroups that are zwitterionic (neutral) include phosphatidylcholine (PC) and phosphatidylethanolamine (PE), while phosphatidylserine (PS), phosphatidic acid (PA), and phosphatidylglycerol (PG) belong to the class of anionic (negatively charged) headgroups.

[20] R. M. Epand, B. Gabel, R. F. Epand, A. Sen, S.-W. Hui, A. Muga, and W. K. Surewicz, Biophys. J. **63**, 327 (1992).

[21] M. Koshinuma, K. Tajima, A. Nakamura, and N. L. Gershfeld, Langmuir **15**, 3430 (1999).

[22] K. A. Riske, R. P. Barroso, C. C. Vequi-Suplicy, R. Germano, V. B. Henriques, and M. T. Lamy, Biochim. Biophys. Acta **1788**, 954 (2009).

[23] R. M. Epand and S.-W. Hui, FEBS Lett. **209**, 257 (1986).

[24] G. Cevc, Chem. Phys. Lipids **64**, 163 (1993).

[25] M. Kodama and T. Miyata, Colloids Surf. A **109**, 283 (1996).

[26] R. Koynova, Chem. Phys. Lipids **89**, 67 (1997).

[27] Y.-P. Zhang, R. N. A. H. Lewis, and R. N. McElhaney, Biophys. J. **72**, 779 (1997).

[28] C. Goldman, K. A. Riske, and M. T. Lamy-Freund, Phys. Rev. E **60**, 7349 (1999); C. Goldman, J. Chem. Phys. **114**, 6242 (2001).

[29] P. A. Forsyth Jr., S. Marčelja, D. J. Mitchell, and B. W. Ninham, Biochim. Biophys. Acta **469**, 335 (1977).

[30] V. Kumaran, Phys. Rev. Lett. **85**, 4996 (2000); W. Sung, E. Choi, and Y. W. Kim, Phys. Rev. E **74**, 031907 (2006); S. Taheri-Araghi and B.-Y. Ha, Langmuir **26**, 14737 (2010).

[31] R. Lipowsky, Nature **349**, 475 (1991); E. Sackmann, FEBS Lett. **346**, 3 (1994); M. M. A. E. Claessens, B. F. van Oort, F. A. M. Leermakers, F. A. Hoekstra, and M. A. C. Stuart, Biophys. J. **87**, 3882 (2004); D. Marsh, Chem. Phys. Lipids **144**, 146 (2006).

[32] X.-J. Li and M. Schick, Biophys. J. **78**, 34 (2000).

[33] S. Komura, H. Shirotori, and T. Kato, J. Chem. Phys. **119**, 1157 (2003).

[34] R. E. Goldstein and S. Leibler, Phys. Rev. Lett. **61**, 2213 (1988); Phys. Rev. A **40**, 1025 (1989).

[35] H. Träuble and H. Eibl, Proc. Natl. Acad. Sci. USA **71**, 214 (1974); F. Jähnig, Biophys. Chem. **4**, 309 (1976); H. Träuble, M. Teubner, P. Woolley, and H. Eibl, *ibid.* **4**, 319 (1976).

[36] A. Watts, K. Harlos, W. Maschke, and D. Marsh, Biochim. Biophys. Acta **510**, 63 (1978).

[37] G. Cevc, A. Watts, and D. Marsh, FEBS Lett. **120**, 267 (1980); Biochemistry **20**, 4955 (1981).

[38] B. R. Copeland and H. C. Andersen, Biochemistry **21**, 2811 (1982).

[39] K. A. Riske, H. G. Döbereiner, and M. T. Lamy-Freund, J. Phys. Chem. B **106**, 239 (2002); **107**, 5391 (2003).

[40] M. Eisenberg, T. Gresalfi, T. Riccio, and S. McLaughlin, Biochemistry **18**, 5213 (1979).

[41] R. Kurland, C. Newton, S. Nir, and D. Papahadjopoulos, Biochim. Biophys. Acta **551**, 137 (1979).

[42] K. Toko and K. Yamafuji, Chem. Phys. Lipids **26**, 79 (1980).

[43] M. E. Loosley-Millman, R. P. Rand, and V. A. Parsegian, Biophys. J. **40**, 221 (1982).

[44] F. Lakhdar-Ghazal, J.-L. Tichadou, and J.-F. Tocanne, Eur. J. Biochem. **134**, 531 (1983).

[45] H. Hauser and G. G. Shipley, Biochemistry **22**, 2171 (1983).

[46] J. Marra, Biophys. J. **50**, 815 (1986).

[47] K. K. Eklund, J. A. Virtanen, K. Vuori, J. Patrikainen, and P. K. J. Kinnunen, Biochemistry **26**, 7542 (1987).

[48] F. Lakhdar-Ghazal and J.-F. Tocanne, Biochim. Biophys. Acta **943**, 19 (1988).

[49] T. I. Lotta, I. S. Salonen, J. A. Virtanen, K. K. Eklund, and P. K. J. Kinnunen, Biochemistry **27**, 8158 (1988).

[50] K. K. Eklund, I. S. Salonen, and P. K. J. Kinnunen, Chem. Phys. Lipids **50**, 71 (1989).

[51] S. McLaughlin, Annu. Rev. Biophys. Biophys. Chem. **18**, 113 (1989).

[52] R. Kraayenhof, G. J. Sterk, H. W. W. F. Sang, K. Krab, and R. M. Epand, Biochim. Biophys. Acta **1282**, 293 (1996).

[53] M. N. Tamashiro, V. B. Henriques, and M. T. Lamy, Langmuir **21**, 11005 (2005).

[54] P. Garidel and A. Blume, Chem. Phys. Lipids **138**, 50 (2005).

[55] Y. Yang, K. M. Mayer, and J. H. Hafner, Biophys. J. **92**, 1966 (2007).

[56] M. Kinoshita, S. Kato, and H. Takahashi, Chem. Phys. Lipids **161**, 1 (2009).

[57] L. A. Meijer, F. A. M. Leermakers, and A. Nelson, Langmuir **10**, 1199 (1994); S. A. Pandit and M. L. Berkowitz, Biophys. J. **82**, 1818 (2002); A. A. Gurtovenko and I. Vattulainen, J. Phys. Chem. B **112**, 4629 (2008).

[58] Y. N. Kaznessis, S. Kim, and R. G. Larson, Biophys. J. **82**, 1731 (2002); K. Murzyn, T. Róg, and M. Pasenkiewicz-Gierula, ibid. **88**, 1091 (2005); D. E. Elmore, FEBS Lett. **580**, 144 (2006); M. Pickholz, O. N. Oliveira Jr., and M. S. Skaf, Biophys. Chem. **125**, 425 (2007); W. Zhao, T. Róg, A. A. Gurtovenko, I. Vattulainen, and M. Karttunen, Biophys. J. **92**, 1114 (2007); Biochimie **90**, 930 (2008); M. Yi, H. Nymeyer, and H.-X. Zhou, Phys. Rev. Lett. **101**, 038103 (2008); J. Hénin, W. Shinoda, and M. L. Klein, J. Phys. Chem. B **113**, 6958 (2009).

[59] S. Doniach, J. Chem. Phys. **68**, 4912 (1978).

[60] A. Caillé, D. Pink, F. de Verteuil, and M. J. Zuckermann, Can. J. Phys. **58**, 581 (1980).

[61] O. G. Mouritsen, A. Boothroyd, R. Harris, N. Jan, T. Lookman, L. MacDonald, D. A. Pink, and M. J. Zuckermann, J. Chem. Phys. **79**, 2027 (1983).

[62] O. G. Mouritsen, Chem. Phys. Lipids **57**, 179 (1991).

[63] R. Jerala, P. F. F. Almeida, and R. L. Biltonen, Biophys. J. **71**, 609 (1996).

[64] I. P. Sugár, T. E. Thompson, and R. L. Biltonen, Biophys. J. **76**, 2099 (1999).

[65] E. I. Michonova-Alexova and I. P. Sugár, Biophys. J. **83**, 1820 (2002).

[66] D. P. Kharakoz, M. S. Panchelyuga, E. I. Tiktopulo, and E. A. Shlyapnikova, Chem. Phys. Lipids **150**, 217 (2007).

[67] J. A. Cohen and M. Cohen, Biophys. J. **36**, 623 (1981); **46**, 487 (1984).

[68] It should be noted that quenched and annealed charge disorder may introduce and/or modify interbilayer interactions between net-neutral surfaces: A. Naydenov, P. A. Pincus, and S. A. Safran, Langmuir **23**, 12016 (2007); R. Brewster, P. A. Pincus, and S. A. Safran, Phys. Rev. Lett. **101**, 128101 (2008); J. Sarabadani, A. Naji, D. S. Dean, R. R. Horgan, and R. Podgornik, J. Chem. Phys. **133**, 174702 (2010); A. Naji, D. S. Dean, J. Sarabadani, R. R. Horgan, and R. Podgornik, Phys. Rev. Lett. **104**, 060601 (2010). However, in our model system, annealed charge disorder occurs only under the condition of electrically charged, non-neutral surfaces, and in that case, monopole interactions should dominate. Furthermore, our interest lies in very dilute aqueous dispersions, for which the effect should be negligible even for *amphoretic* net-neutral surfaces, in which oppositely charged headgroups are randomly distributed. Moreover, for amphoretic non-neutral surfaces, it has been proposed in a very recent study, H. T. Baytekin, A.

Z. Patashinski, M. Branicki, B. Baytekin, S. Soh, and B. A. Grzybowski, Science **333**, 308 (2011), that the underlying physical mechanism behind the very old problem of contact electrification in dielectric materials is the development of a random mosaic of oppositely charged regions of nanoscopic dimensions.

[69] This counterion adsorption to the phospholipid headgroups is mediated by the aqueous solvent and should be classified as *physisorption*, in contrast to *chemisorption*, in which there is a chemical bound: *IUPAC, Compendium of Chemical Terminology* (the "Gold Book"), 2nd ed., compiled by A. D. McNaught and A. Wilkinson (Blackwell Scientific, Oxford, 1997). XML on-line corrected versions at http://goldbook.iupac.org/C01048.html and http://goldbook.iupac.org/P04667.html. This standard discrimination, however, has recently been challenged, as the distinction between them is somewhat arbitrary: J. Lyklema, Colloids Surf. A **291**, 3 (2006); Adv. Colloid Interface Sci. **147-148**, 205 (2009); A. Travesset and S. Vangaveti, J. Chem. Phys. **131**, 185102 (2009).

[70] R. R. Netz, Phys. Rev. E **60**, 3174 (1999).

[71] Y. Levin, Phys. Rev. Lett. **102**, 147803 (2009); Y. Levin, A. P. dos Santos, and A. Diehl, ibid. **103**, 257802 (2009); A. P. dos Santos, A. Diehl, and Y. Levin, Langmuir **26**, 10778 (2010); A. P. dos Santos and Y. Levin, J. Chem. Phys. **133**, 154107 (2010).

[72] M. N. Tamashiro and M. A. Constantino, J. Phys. Chem. B **114**, 3583 (2010).

[73] G. Cevc and D. Marsh, J. Phys. Chem. **87**, 376 (1983); D. Ben-Yaakov, D. Andelman, and R. Podgornik, J. Chem. Phys. **134**, 074705 (2010).

[74] T. D. Lee and C. N. Yang, Phys. Rev. **87**, 410 (1952); R. J. Baxter, *Exactly Solved Models in Statistical Mechanics* (Academic Press, London, 1982), Sec. 1.9, p. 24; H. E. Stanley, *Introduction to Phase Transitions and Critical Phenomena* (Clarendon Press, Oxford, 1971), App. A, p. 260.

[75] J. Oitmaa, J. Phys. A **14**, 1159 (1981); D. P. Landau and K. Binder, Phys. Rev. B **31**, 5946 (1985).

[76] A. Tröster, Phys. Rev. B **81**, 012406 (2010).

[77] J. Ashkin and E. Teller, Phys. Rev. **64**, 178 (1943); R. V. Ditzian, J. R. Banavar, G. S. Grest, and L. P. Kadanoff, Phys. Rev. B **22**, 2542 (1980).

[78] P. Pawlicki and J. Rogiers, Physica A **214**, 277 (1995); P. Pawlicki, G. Musial, G. Kamieniarz, and J. Rogiers, ibid. **242**, 281 (1997).

[79] L. K. Nielsen, T. Bjørnholm, and O. G. Mouritsen, Nature **404**, 352 (2000); Langmuir **23**, 11684 (2007).

[80] S. Doniach, J. Chem. Phys. **70**, 4587 (1979); M. Marder, H. L. Frisch, J. S. Langer, and H. M. McConnell, Proc. Natl. Acad. Sci. USA **81**, 6559 (1984); J. M. Carlson and J. P. Sethna, Phys. Rev. A **36**, 3359 (1987); W. S. McCullough and H. L. Scott, Phys. Rev. Lett. **65**, 931 (1990); G. Cevc, Biochim. Biophys. Acta **1062**, 59 (1991); T. C. Lubensky and F. C. MacKintosh, Phys. Rev. Lett. **71**, 1565 (1993); S. Kirchner and G. Cevc, Europhys. Lett. **28**, 31 (1994); W.-J. Sun, S. Tristram-Nagle, R. M. Suter, and J. F. Nagle, Proc. Natl. Acad. Sci. USA **93**, 7008 (1996); T. Heimburg, Biophys. J. **78**, 1154 (2000).

[81] L. Néel, Ann. Phys. (Paris) **3**, 137 (1948); R. J. Baxter, *Exactly Solved Models in Statistical Mechanics* (Academic Press, London, 1982), Chap. 4, p. 47; C. J. Thompson, J. Stat. Phys. **27**, 441 (1982).

[82] B. H. Zimm and M. Le Bret, J. Biomol. Struct. Dyn. **1**, 461 (1983) [PMID 6400884] [http://www.ncbi.nlm.nih.gov/pubmed/6400884]; G. Lamm and G. R. Pack, Biopolymers **93**, 619 (2010).

[83] C. J. Thompson, *Classical Equilibrium Statistical Mechanics* (Clarendon Press, Oxford, 1988), Sec. 4.3, p. 91; S. R. A. Salinas, *Introduction to Statistical Physics* (Springer-Verlag, New York, 2001), Sec. 13.3, p. 266.

[84] J. L. Lebowitz and O. Penrose, J. Math. Phys. **7**, 98 (1966); T. Mori, Phys. Rev. E **82**, 060103(R) (2010).

[85] Due to the effective antiferromagnetic coupling $-\upsilon < 0$ between the $\{\tau_i\}$ variables, the thermodynamic free energy ψ_{2N} *is not a minimum* of the functional Ψ_{2N} with respect to $\mathbf{r}$. However, the thermodynamic stable solution is given by the extremum of $\Psi_{2N}(\mathbf{r})$ associated with the lowest free energy. See, e.g., the discussion for the simplest case of an Ising antiferromagnet, R. Agra, F. van Wijland, and E. Trizac, Eur. J. Phys. **27**, 407 (2006).

[86] In fact, Eq. (25) is still a free-energy *functional*. In particular, it is not possible to attribute a physical interpretation to the several contributions of Eq. (25), as discussed for the specific case of the ferromagnetic Ising model in C. E. I. Carneiro, V. B. Henriques, and S. R. Salinas, Physica A **162**, 88 (1989).

[87] Incidentally, one should mention that a proper definition of the mechanical lateral pressure Π for unilamellar vesicles is a nontrivial question: C. Tanford, Proc. Natl. Acad. Sci. USA **76**, 3318 (1979); S. H. White, *ibid.* **77**, 4048 (1980); L. J. Lis, M. McAlister, N. Fuller, R. P. Rand, and V. A. Parsegian, Biophys. J. **37**, 667 (1982) [PMID 7074192] [http://www.ncbi.nlm.nih.gov/pubmed/7074192], [PMCID PMC1328852] [http://www.ncbi.nlm.nih.gov/pmc/articles/PMC1328852]; S.-s. Feng, Langmuir **15**, 998 (1999); D. Marsh, *ibid.* **22**, 2916 (2006); J.-B. Fournier and C. Barbetta, Phys. Rev. Lett. **100**, 078103 (2008); C. Barbetta, A. Imparato, and J.-B. Fournier, Eur. Phys. J. E **31**, 333 (2010).

[88] V. B. Henriques, R. Germano, M. T. Lamy, and M. N. Tamashiro, Phase transitions and spatially ordered counterion association in ionic-lipid membranes: theory versus experiment, Langmuir, doi: 10.1021/la202302x (to be published).

[89] C. A. Helm, L. Laxhuber, M. Lösche, and H. Möhwald, Colloid Polym. Sci. **264**, 46 (1986); G. Cevc, Biochim. Biophys. Acta **1031**, 311 (1990); H. Hauser, Chem. Phys. Lipids **57**, 309 (1991).

[90] We should note that our calculations were performed, for mathematical convenience, at *fixed* lateral pressure Π. Although this condition may not be satisfied in experimental measurements in ionic-lipid suspensions, there is evidence, however, that monolayers and bilayers are equivalent at a lateral pressure Π between 30 mN/m and 35 mN/m, which would correspond to the tension-free state normally found in extended lipid bilayers: A. Blume, Biochim. Biophys. Acta **557**, 32 (1979); D. Marsh, *ibid.* **1286**, 183 (1996).

[91] J. L. Ranck, T. Keira, and V. Luzzati, Biochim. Biophys. Acta **488**, 432 (1977); P. Garidel, W. Richter, G. Rapp, and A. Blume, Phys. Chem. Chem. Phys. **3**, 1504 (2001).

[92] G. H. Wannier, Phys. Rev. **79**, 357 (1950); correction: Phys. Rev. B **7**, 5017 (1973); R. M. F. Houtappel, Physica **16**, 425 (1950); C. Domb, Adv. Phys. **9**, 149 (1960); C. Domb, in *Phase Transitions and Critical Phenomena*, edited by C. Domb and M. S. Green (Academic Press, London, 1974), Vol. 3, Chap. 6, p. 357; M. N. Tamashiro and S. R. Salinas, Phys. Rev. B **56**, 8241 (1997); S. L. A. de Queiroz, T. Paiva, J. S. de Sá Martins, and R. R. dos Santos, Phys. Rev. E **59**, 2772 (1999); C. Moore, M. G. Nordahl, N. Minar, and C. R. Shalizi, *ibid.* **60**, 5344 (1999); A. Pelizzola and M. Pretti, Phys. Rev. B **60**, 10134 (1999); S. Galam and P.-V. Koseleff, Eur. Phys. J. B **28**, 149 (2002); X. Qian, M. Wegewijs, and H. W. J. Blöte, Phys. Rev. E **69**, 036127 (2004); R. P. Millane and R. M. Clare, *ibid.* **74**, 051101 (2006); Y. Han, Y. Shokef, A. M. Alsayed, P. Yunker, T. C. Lubensky, and A. G. Yodh, Nature **456**, 898 (2008); K. Katsumata, H. A. Katori, S. Kimura, Y. Narumi, M. Hagiwara, and K. Kindo, Phys. Rev. B **82**, 104402 (2010).

[93] P. R. Cullis and B. de Kruijff, Biochim. Biophys. Acta **559**, 399 (1979); R. Koynova and M. Caffrey, Chem. Phys. Lipids **115**, 107 (2002); L. van Dam, G. Karlsson, and K. Edwards, Biochim. Biophys. Acta **1664**, 241 (2004); J. Katsaras, T. A. Harroun, J. Pencer, and M.-P. Nieh, Naturwissenschaften **92**, 355 (2005).

[94] J. N. Israelachvili, *Intermolecular and Surface Forces*, 2nd ed. (Academic Press, London, 1992), Chap. 12, p. 213; D. Andelman, in *Handbook of Biological Physics*, edited by R. Lipowsky and E. Sackmann (Elsevier, Amsterdam, 1995), Vol. 1B, Chap. 12, p. 603; R. R. Netz and H. Orland, Eur. Phys. J. E **1**, 203 (2000); M. Deserno and C. Holm, in *Proceedings of the NATO Advanced Study Institute on Electrostatic Effects in Soft Matter and Biophysics*, edited by C. Holm, P. Kékicheff, and R. Podgornik (Kluwer, Dordrecht, 2001), p. 27; S. A. Safran, *Statistical Thermodynamics of Surfaces, Interfaces and Membranes* (Addison-Wesley, Reading, MA, 1994), Sec. 5.5, p. 153; M. N. Tamashiro and H. Schiessel, Phys. Rev. E **68**, 066106 (2003); G. Lamm, Rev. Comp. Ch. **19**, 147 (2003); P. Grochowski and J. Trylska, Biopolymers **89**, 93 (2007).

[95] D. Harries, R. Podgornik, V. A. Parsegian, E. Mar-Or, and D. Andelman, J. Chem. Phys. **124**, 224702 (2006).

[96] Y. S. Jho, M. W. Kim, S. A. Safran, and P. A. Pincus, Eur. Phys. J. E **31**, 207 (2010).

[97] E. Leontidis, A. Aroti, L. Belloni, M. Dubois, and T. Zemb, Biophys. J. **93**, 1591 (2007).

[98] E. Leontidis, A. Aroti, and L. Belloni, J. Phys. Chem. B **113**, 1447 (2009).